Learning to Augment Distributions for
Out-of-Distribution Detection

Qizhou Wang[1]*   Zhen Fang[2]*   Yonggang Zhang[1]   Feng Liu[3]   Yixuan Li[4]   Bo Han[1]†

[1]Department of Computer Science, Hong Kong Baptist University
[2]Australian Artificial Intelligence Institute, University of Technology Sydney
[3]School of Computing and Information Systems, The University of Melbourne
[4]Department of Computer Sciences, University of Wisconsin-Madison
{csqzwang, csygzhang, bhanml}@comp.hkbu.edu.hk
zhen.fang@uts.edu.au   fengliu.ml@gmail.com   sharonli@cs.wisc.edu

Abstract

Open-world classification systems should discern out-of-distribution (OOD) data whose labels deviate from those of in-distribution (ID) cases, motivating recent studies in OOD detection. Advanced works, despite their promising progress, may still fail in the open world, owing to the lack of knowledge about unseen OOD data in advance. Although one can access auxiliary OOD data (distinct from unseen ones) for model training, it remains to analyze how such auxiliary data will work in the open world. To this end, we delve into such a problem from a learning theory perspective, finding that the distribution discrepancy between the auxiliary and the unseen real OOD data is the key to affecting the open-world detection performance. Accordingly, we propose *Distributional-Augmented OOD Learning* (DAL), alleviating the OOD distribution discrepancy by crafting an *OOD distribution set* that contains all distributions in a Wasserstein ball centered on the auxiliary OOD distribution. We justify that the predictor trained over the worst OOD data in the ball can shrink the OOD distribution discrepancy, thus improving the open-world detection performance given only the auxiliary OOD data. We conduct extensive evaluations across representative OOD detection setups, demonstrating the superiority of our DAL over its advanced counterparts. The code is publicly available at: https://github.com/tmlr-group/DAL.

1 Introduction

Deep learning in the open world often encounters out-of-distribution (OOD) data of which the label space is disjoint with that of the in-distribution (ID) cases (Hendrycks and Gimpel, 2017; Fang et al., 2022). It leads to the well-known OOD detection problem, where the predictor should make accurate predictions for ID data and detect anomalies from OOD cases (Bulusu et al., 2020; Yang et al., 2021). Nowadays, OOD detection has attracted intensive attention in reliable machine learning due to its integral role in safety-critical applications (Cao et al., 2020; Shen et al., 2021).

OOD detection remains challenging since predictors can make over-confidence predictions for OOD data (Hendrycks et al., 2019), motivating recent studies towards effective OOD detection. Therein, outlier exposure (Hendrycks et al., 2019; Ming et al., 2022) is among the most potent ones, learning from *auxiliary OOD data* to discern ID and OOD patterns. However, due to the openness of the OOD task objective (Wang et al., 2023), auxiliary OOD data can arbitrarily differ from the (unseen) real OOD data in the open world. So, to formally understand their consequences, we model the difference

---

*Equal contributions.
†Correspondence to Bo Han (bhanml@comp.hkbu.edu.hk).

between auxiliary and real OOD data by their distribution discrepancy, measured by the Wasserstein distance (Villani, 2021, 2008). Then, we reveal the negative impacts of such OOD distribution discrepancy on the real detection power, with a larger distribution discrepancy indicating a lower performance on real OOD data, cf., Eq. (4).

The OOD distribution discrepancy threatens the open-world detection performance for outlier exposure. Therefore, we raise a natural question in *how to alleviate such an OOD distribution discrepancy*. Hence, this paper establishes a promising learning framework named *Distributional-Augmented OOD Learning* (DAL). Therein, we augment the auxiliary OOD distribution by crafting an *OOD distribution set* containing all distributions in a Wasserstein ball (Villani, 2021, 2008), centered on the auxiliary OOD distribution. Then, by making the predictor learn from the worst OOD distribution in the set, cf., Eq. (8), one can alleviate the negative impacts of the distribution discrepancy. Moreover, our proposed framework enjoys the learning guarantees towards the expected risk with respect to the real OOD distribution, making OOD detection stay effective when facing unseen data (cf., Theorem 3). Figure 1 provides a conceptual explanation: learning from the worst OOD distribution ensures the uniformly well performance inside the Wasserstein ball, enlarging the influence of the auxiliary OOD distribution. Thus, one can shrink the OOD distribution discrepancy between the auxiliary and the real OOD data and improve OOD detection.
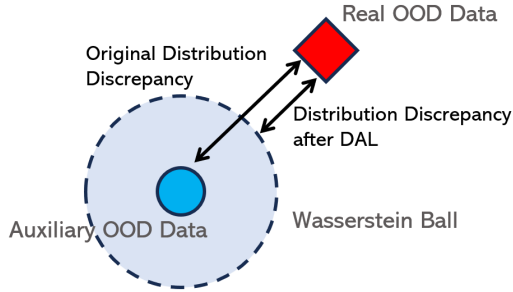

Figure 1: A heuristic illustration for our DAL. A large distribution discrepancy between the auxiliary and the unseen OOD data will hurt the real detection effectiveness. However, by ensuring uniformly well performance inside the Wasserstein ball, we can mitigate the distribution discrepancy and thus improve the detection power in the open world.

In realization, the primal learning objective in Eq. (8) is generally intractable due to the infinite-dimensional optimization for the worst OOD distribution search. Instead, we adopt the dual form with respect to the original learning problem (cf., Theorem 1), transforming it into a tractable problem of the worst OOD data search in a finite-dimensional space. Furthermore, following Du et al. (2022a); Mehra et al. (2022), the data search procedure is conducted in the embedding space, which can benefit the open-world performance of OOD detection with decent costs of additional computation.

We conduct extensive experiments over representative OOD detection setups, revealing the open-world performance of our method toward effective OOD detection. For example, our DAL reduces the average FPR95 by 1.99 to 13.46 on CIFAR benchmarks compared with the conventional outlier exposure (Hendrycks et al., 2019). Overall, we summarize our contributions into three folds:

- We measure the difference between the auxiliary and the real OOD data by the Wasserstein distance, and establish an effective learning framework, named DAL, to mitigate the OOD distribution discrepancy issue. We further guarantee our performance with respect to unseen real OOD data via Theorem 3, which is new to previous works.

- DAL leads to a practical method in Algorithm 1, learning from the worst cases in the Wasserstein ball to improve the open-world detection performance. Overall, our method solves the dual problem, which performs the worst-case search in the embedding space, which is simple to compute yet effective in OOD detection.

- We conduct extensive experiments in Section 5 to evaluate our effectiveness, ranging from the well-known CIFAR benchmarks to the challenging ImageNet settings. The empirical results comprehensively demonstrate our superiority over advanced counterparts, and the improvement is mainly attributed to our distributional-augmented learning framework.

A detailed overview of existing OOD detection methods and theories can be found in Appendix A, and a summary of the important notations can be found in Appendix B.

2   Outlier Exposure

Let $\mathcal{X}$ denote the feature space and $\mathcal{Y} = \{1, \ldots, C\}$ denote the label space with respect to the ID distribution. We consider the ID distribution $D_{X_I Y_I}$, a joint distribution defined over $\mathcal{X} \times \mathcal{Y}$, where X_I and Y_I are random variables whose outputs are from spaces $\mathcal{X}$ and $\mathcal{Y}$. We also have an OOD joint distribution $D_{X_O Y_O}$, where X_O is a random variable from $\mathcal{X}$, but Y_O is a random variable whose outputs do not belong to $\mathcal{Y}$, i.e., $Y_O \notin \mathcal{Y}$ (Fang et al., 2022).

The classical OOD detection (Hendrycks and Gimpel, 2017; Yang et al., 2021) typically considers an open-world setting, where the real OOD data drawn from $D_{X_O Y_O}$ are unseen during training. Recently, Fang et al. (2022) have provided several *strong* conditions necessary to ensure the success of the classical OOD setting. Furthermore, to increase the possibility of success for OOD detection and weaken the strong conditions proposed by Fang et al. (2022), advanced works (Hendrycks et al., 2019; Chen et al., 2021) introduce a promising approach named *outlier exposure*, where a set of auxiliary OOD data is employed as a surrogate of real OOD data. Here, we provide a formal definition.

Problem 1 (OOD Detection with Outlier Exposure). Let $D_{X_I Y_I}$, D_{X_O}, and D_{X_A} be the ID joint distribution, the OOD distribution, and the auxiliary OOD distribution, respectively. Given the sets of samples called the ID and the auxiliary OOD data, namely,

$$S = \{(\mathbf{x}_I^1, y_I^1), \ldots, (\mathbf{x}_I^n, y_I^n)\} \sim D_{X_I Y_I}^n, \ i.i.d., \quad T = \{\mathbf{x}_A^1, \ldots, \mathbf{x}_A^m\} \sim D_{X_A}^m, \ i.i.d.,$$

outlier exposure trains a predictor $\mathbf{f}$ by using the training data S and T, such that for any test data $\mathbf{x}$:
1) if $\mathbf{x}$ is an observation from D_{X_I}, the predictor $\mathbf{f}$ can classify $\mathbf{x}$ into its correct ID label; otherwise
2) if $\mathbf{x}$ is an observation from D_{X_O}, the predictor $\mathbf{f}$ can detect $\mathbf{x}$ as an OOD case.

OOD Scoring. Many existing methods detect OOD data by using various score-based strategies (Hendrycks and Gimpel, 2017; Lee et al., 2018a; Liu et al., 2020; Sun et al., 2022). In general, given a model $\mathbf{f} : \mathcal{X} \to \mathbb{R}^C$ and a scoring function $s(\cdot; \mathbf{f}) : \mathcal{X} \to \mathbb{R}$, the OOD detector g_λ is given by:

$$g_\lambda(\mathbf{x}) = \text{ID}, \ \text{if } s(\mathbf{x}; \mathbf{f}) \geq \lambda; \text{ otherwise, } g_\lambda(\mathbf{x}) = \text{OOD},$$

where λ is a given threshold. For example, as a well-known baseline scoring function, the maximum softmax prediction (MSP) (Hendrycks and Gimpel, 2017) is given by:

$$s_{\text{MSP}}(\mathbf{x}; \mathbf{f}) = \max_{k \in \mathcal{Y}} \mathtt{softmax}_k \, \mathbf{f}(\mathbf{x}), \tag{1}$$

with $\mathtt{softmax}_k(\cdot)$ denoting the k-th dimension of the softmax output.

Model and Risks. We denote $\mathbf{f_w} : \mathcal{X} \to \mathbb{R}^C$ the predictor with parameters $\mathbf{w} \in \mathcal{W}$, with $\mathcal{W}$ the parameter space. We consider the loss functions ℓ and ℓ_{OE} w.r.t. the ID and the OOD cases, respectively. Then, the expected and the empirical *ID risks* of the model $\mathbf{f_w}$ can be written as:

$$R_I(\mathbf{w}) = \mathbb{E}_{(\mathbf{x}, y) \sim D_{X_I Y_I}} \ell(\mathbf{f_w}; \mathbf{x}, y) \ \text{and} \ \widehat{R}_I(\mathbf{w}) = \frac{1}{n} \sum_{i=1}^n \ell(\mathbf{f_w}; \mathbf{x}_I^i, y_I^i).$$

The expected and the empirical *auxiliary OOD risks* are then given by

$$R_A(\mathbf{w}) = \mathbb{E}_{\mathbf{x} \sim D_{X_A}} \ell_{\text{OE}}(\mathbf{f_w}; \mathbf{x}) \ \text{and} \ \widehat{R}_A(\mathbf{w}) = \frac{1}{m} \sum_{i=1}^m \ell_{\text{OE}}(\mathbf{f_w}; \mathbf{x}_A^i),$$

and the expected *real OOD risk* is given by $R_O(\mathbf{w}) = \mathbb{E}_{\mathbf{x} \sim D_{X_O}} \ell_{\text{OE}}(\mathbf{f_w}; \mathbf{x})$. Accordingly, we can define the expected *detection risk* with respect to real OOD data, following

$$R_D(\mathbf{w}) = R_I(\mathbf{w}) + \alpha R_O(\mathbf{w}), \tag{2}$$

where α is the trade-off parameter.

Learning Strategy. After the scoring function is selected, one can obtain the OOD detector if the model $\mathbf{f_w}$ is given. Under the Problem 1 of outlier exposure, a common learning strategy is to optimize the empirical ID and auxiliary OOD risk jointly (Hendrycks et al., 2019), namely,

$$\min_{\mathbf{w} \in \mathcal{W}} \left[\widehat{R}_I(\mathbf{w}) + \alpha \widehat{R}_A(\mathbf{w}) \right]. \tag{3}$$

Note that the auxiliary OOD data are employed in Eq. (3), which can arbitrarily differ from the real OOD cases. Then, it is generally expected that the predictor $\mathbf{f_w}$, trained over the auxiliary OOD data, can perform well even on unseen OOD data, i.e., a small value of $R_D(\mathbf{w})$ is expected.

3 Motivation

To the general learning strategy in Eq. (3), intuitively, if the auxiliary data are sampled from a distribution similar to real ones, the predictor will perform well for real OOD data. However, auxiliary and real OOD data differ in practice, posing us to suspect their open-world detection performance. To formally study the problem, we measure the difference between auxiliary and real OOD data in the distribution level, motivating our discussion of *OOD distribution discrepancy*.

Distribution Discrepancy. In this paper, we adopt a classical measurement for the distribution discrepancy—Optimal Transport Cost (Sinha et al., 2018; Mehra et al., 2022).

Definition 1 (Optimal Transport Cost and Wasserstein-1 Distance (Villani, 2021, 2008)). Given a cost function $c : \mathcal{X} \times \mathcal{X} \to \mathbb{R}_+$, the *optimal transport cost* between two distributions D and D' is

$$\mathrm{W}_c(D, D') = \inf_{\pi \in \Pi(D,D')} \mathbb{E}_{(\mathbf{x},\mathbf{x}') \sim \pi} c(\mathbf{x}, \mathbf{x}'),$$

where $\Pi(D, D')$ is the space of all couplings for D and D'. Furthermore, if the cost c is a *metric*, then the optimal transport cost is also called the *Wasserstein-1* distance.

Based on Definition 1, we use the distribution discrepancy to measure the difference between the auxiliary and the real OOD data, namely, $\mathrm{W}_c(D_{X_O}, D_{X_A})$. Then, we can formally study the impacts of such a discrepancy on the detection performance of the predictor. Under certain assumptions (cf., Corollary 1), we can prove that with high probability, the following generalization bound holds:

$$R_D(\widehat{\mathbf{w}}) \leq \min_{\mathbf{w} \in \mathcal{W}} (R_I(\mathbf{w}) + \alpha R_A(\mathbf{w})) + \alpha L_c \mathrm{W}_c(D_{X_O}, D_{X_A}) + \mathcal{O}(1/\sqrt{n}) + \mathcal{O}(1/\sqrt{m}), \quad (4)$$

where $\widehat{\mathbf{w}}$ is the parameter learned by Eq. (3), i.e., $\widehat{\mathbf{w}} \in \arg\min_{\mathbf{w} \in \mathcal{W}} \widehat{R}_I(\mathbf{w}) + \alpha \widehat{R}_A(\mathbf{w})$, L_c is the Lipschitz constant of ℓ_{OE} w.r.t. the cost function $c(\cdot, \cdot)$ (see Theorem 3). In general, the expected detection risk $R_D(\widehat{\mathbf{w}})$ measures the expected performance on unseen OOD data given the predictor trained on the auxiliary OOD data. Then, due to the upper bound, the impacts of the OOD distribution discrepancy are reflected by the Wasserstein-1 distance between the auxiliary and the real OOD data, i.e., $\mathrm{W}_c(D_{X_O}, D_{X_A})$. Therefore, although classical outlier exposure can improve OOD detection to some extent, it fails to ensure reliable detection of unseen OOD data, in that a larger distribution discrepancy generally indicates a worse guarantee for open-world OOD detection.

The key to improve the detection performance is mitigating the negative impact induced by the OOD distribution discrepancy. To tackle this problem, a simple lemma inspires us:

Lemma 1. *Let $d(\cdot, \cdot)$ be the distance to measure the discrepancy between distributions. Given a space $\mathfrak{D}$ consisting of some OOD distributions, if $D_{X_A} \in \mathfrak{D}$, then*

$$\inf_{D_{X'} \in \mathfrak{D}} d(D_{X'}, D_{X_O}) \leq d(D_{X_A}, D_{X_O}). \quad (5)$$

If $d(\cdot, \cdot)$ is the Optimal Transport Cost in Definition 1, the cost function c is a continuous metric, and $\mathfrak{D}$ is the Wasserstein-1 ball with a radius $\rho > 0$, i.e., $\mathfrak{D} = \{D_{X'} : \mathrm{W}_c(D_{X'}, D_{X_A}) \leq \rho\}$, then

$$\inf_{D_{X'} \in \mathfrak{D}} \mathrm{W}_c(D_{X'}, D_{X_O}) \leq \max\{\mathrm{W}_c(D_{X_A}, D_{X_O}) - \rho, 0\}. \quad (6)$$

In the light of Lemma 1, we introduce a specific set of distributions $\mathfrak{D}$, augmented around the auxiliary OOD distribution. It makes it possible to mitigate the distribution discrepancy, following Eqs. (5) and (6). Therefore, instead of choosing a model $\mathbf{f_w}$ that directly minimizes the empirical risk in Eq. (3), we target augmenting the auxiliary OOD data within the distribution space $\mathfrak{D}$, namely,

$$\min_{\mathbf{w} \in \mathcal{W}} \left[\widehat{R}_I(\mathbf{w}) + \alpha \sup_{D_{X'} \in \mathfrak{D}} \mathbb{E}_{\mathbf{x} \sim D_{X'}} \ell_{OE}(\mathbf{f_w}; \mathbf{x}) \right], \text{ subject to } \widehat{D}_{X_A} \in \mathfrak{D}, \quad (7)$$

where $\widehat{D}_{X_A}$ is the empirical form of D_{X_A}, i.e., $\widehat{D}_{X_A} = \frac{1}{m} \sum_{i=1}^{m} \delta_{\mathbf{x}_A^i}$ and $\delta_{\mathbf{x}_A^i}$ is the dirac measure.

4 Learning Framework

This section proposes a general learning framework to mitigate the OOD distribution discrepancy. As aforementioned, we consider an augmented set of OOD distributions to improve OOD detection, thus named *Distributional-Augmented OOD Learning* (DAL).

To begin with, we need to select a suitable distribution space $\mathfrak{D}$ for the tractable solutions of Eq. (7). Generally, the choice of $\mathfrak{D}$ influences both the richness of the auxiliary data as well as the tractability of the resulting optimization problem. Previous works have developed a series of distribution spaces, e.g., the distribution ball based on f-divergences (Namkoong and Duchi, 2016; Michel et al., 2021) and maximum mean discrepancy (MMD) (Staib and Jegelka, 2019). However, there are several drawbacks for the distribution balls based on f-divergences and MMD: 1) any f-divergence-based space $\mathfrak{D}$ contains only distributions within the same support set as $\widehat{D}_{X_A}$; and 2) the effective solutions in the MMD-based space have not been provided (Staib and Jegelka, 2019).

Instead, motivated by Sinha et al. (2018); Mehra et al. (2022); Dai et al. (2023) and Theorem 1, we consider the Wasserstein ball. For any $\rho > 0$, we define the augmented OOD distribution set as

$$\mathfrak{D} = \{D_{X'} : W_c(D_{X'}, \widehat{D}_{X_A}) \leq \rho\},$$

and consider the following optimization problem:

$$\min_{\mathbf{w} \in \mathcal{W}} \widehat{R}_D(\mathbf{w}; \rho) = \min_{\mathbf{w} \in \mathcal{W}} \left[\widehat{R}_I(\mathbf{w}) + \alpha \widehat{R}_O(\mathbf{w}; \rho) \right], \tag{8}$$

where

$$\widehat{R}_O(\mathbf{w}; \rho) = \sup_{W_c(D_{X'}, \widehat{D}_{X_A}) \leq \rho} \mathbb{E}_{\mathbf{x} \sim D_{X'}} \ell_{OE}(\mathbf{f_w}; \mathbf{x}). \tag{9}$$

However, the optimization problem in Eq. (8) is intractable due to the infinite-dimensional search for the distribution $D_{X'}$. Fortunately, the following dual theorem provides a solution:

Theorem 1 (Blanchet and KarthyekRajhaaA. (2016))**.** *Let $c(\cdot, \cdot)$ be a continuous metric and $\phi_\gamma(\mathbf{w}; \mathbf{x}) = \sup_{\mathbf{x}' \in \mathcal{X}} \{\ell(\mathbf{f_w}; \mathbf{x}') - \gamma c(\mathbf{x}', \mathbf{x})\}$ be the robust surrogate function. Then, for any $\rho > 0$,*

$$\widehat{R}_D(\mathbf{w}; \rho) = \widehat{R}_I(\mathbf{w}) + \alpha \inf_{\gamma \geq 0} \left\{ \gamma \rho + \frac{1}{m} \sum_{i=1}^{m} \phi_\gamma(\mathbf{w}; \mathbf{x}_A^i) \right\}. \tag{10}$$

Theorem 1 provides a feasible surrogate for the original optimization problem in Eq. (8), transforming the infinite-dimensional problem to its finite counterpart, i.e., the data feature search. We use Eq. (10) to design our algorithm, cf., Section 4.2.

4.1 Theoretical Supports

This section provides the theoretical support for our DAL. Specifically, 1) Theorem 2 shows that the empirical model given by Eq. (8) can achieve consistent learning performance, and 2) Theorem 3 further demonstrates the expected detection risk estimation, i.e., $R_D(\mathbf{w})$, with respect to the empirical model given by Eq. (8). All the proofs can be found in Appendix C. To state our theoretical results, we use the notation $R_D(\mathbf{w}; \rho)$ to represent the ideal form of $\widehat{R}_D(\mathbf{w}; \rho)$, which is defined by

$$R_D(\mathbf{w}; \rho) = R_I(\mathbf{w}) + \alpha R_O(\mathbf{w}; \rho),$$

where

$$R_O(\mathbf{w}; \rho) = \sup_{W_c(D_{X'}, D_{X_A}) \leq \rho} \mathbb{E}_{\mathbf{x} \sim D_{X'}} \ell_{OE}(\mathbf{f_w}; \mathbf{x}).$$

Similar to Sinha et al. (2018), our results rely on the covering number (cf., Appendix C.1) for the model classes $\mathcal{F} = \{\ell(\mathbf{f_w}; \cdot) : \mathbf{w} \in \mathcal{W}\}$ and $\mathcal{F}_{OE} = \{\ell_{OE}(\mathbf{f_w}; \cdot) : \mathbf{w} \in \mathcal{W}\}$ to represent their complexity. Intuitively, the covering numbers $\mathcal{N}(\mathcal{F}, \epsilon, L^\infty)$ and $\mathcal{N}(\mathcal{F}_{OE}, \epsilon, L^\infty)$ are the minimal numbers of L^∞ balls of radius $\epsilon > 0$ needed to cover the model classes $\mathcal{F}$ and $\mathcal{F}_{OE}$, respectively. Now, we demonstrate that DAL can achieve consistent performance under mild assumptions.

Theorem 2 (Excess Generalization Bound)**.** *Assume that $0 \leq \ell(\mathbf{f_w}; \mathbf{x}, y) \leq M_\ell$, $0 \leq \ell_{OE}(\mathbf{f_w}; \mathbf{x}) \leq M_{\ell_{OE}}$, and $c(\cdot, \cdot) : \mathcal{X} \times \mathcal{X} \to \mathbb{R}_+$ is a continuous metric. Let $\widehat{\mathbf{w}}$ be the optimal solution of Eq. (8), i.e., $\widehat{\mathbf{w}} \in \arg\min_{\mathbf{w} \in \mathcal{W}} \widehat{R}_D(\mathbf{w}; \rho)$. Then with the probability at least $1 - 4e^{-t} > 0$,*

$$R_D(\widehat{\mathbf{w}}; \rho) - \min_{\mathbf{w} \in \mathcal{W}} R_D(\mathbf{w}; \rho) \leq \epsilon(n, m; t), \tag{11}$$

for any $\rho > 0$, where

$$\epsilon(n, m; t) = \frac{b_0 M_\ell}{\sqrt{n}} \int_0^1 \sqrt{\log \mathcal{N}(\mathcal{F}, M_\ell \epsilon, L^\infty)} d\epsilon + 2M_\ell \sqrt{\frac{2t}{n}}$$

$$+ \alpha b_1 \sqrt{\frac{M_{\ell_{OE}}^3}{\rho^2 m}} \int_0^1 \sqrt{\log \mathcal{N}(\mathcal{F}_{OE}, M_{\ell_{OE}} \epsilon, L^\infty)} d\epsilon + \alpha b_2 M_{\ell_{OE}} \sqrt{\frac{2t}{m}},$$

where b_0, b_1 and b_2 are uniform constants.

5

Algorithm 1 Distributional-Augmented OOD Learning (DAL)

Input: ID and OOD samples from $D_{X_I Y_I}$ and D_{X_A};

for st $= 1$ **to** num_step **do**

    Sample S_B and T_B from $D_{X_I Y_I}$ and D_{X_A};

    Initialize $\mathbf{p}^i \sim \mathcal{N}(\mathbf{0}, \sigma I)$, $\forall\, i \in \{1, \ldots, |T_B|\}$;

    for se $= 1$ **to** num_search **do**

        $\boldsymbol{\psi}^i = \nabla_{\mathbf{p}^i}\left[\ell_{\mathrm{OE}}\left(\mathbf{h}(\mathbf{e}(\mathbf{x}_A^i + \mathbf{p}^i); \mathbf{e}(\mathbf{x}_A^i)\right) - \gamma \left\|\mathbf{p}^i\right\|_1\right]$, $\forall\, i \in \{1, \ldots, |T_B|\}$;

        $\mathbf{p}^i \leftarrow \mathbf{p}^i + \mathrm{ps}\boldsymbol{\psi}^i$, $\forall\, i \in \{1, \ldots, |T_B|\}$

    end for

    $\gamma \leftarrow \min\left(\max\left(\gamma - \beta(\rho - \frac{1}{|T_B|}\sum_{i=1}^{|T_B|}\|\mathbf{p}^i\|, \gamma_{\max}\right), 0\right)$;

    $\mathbf{w} \leftarrow \mathbf{w} - \mathrm{lr}\nabla_{\mathbf{w}}\left[\frac{1}{|T_B|}\sum_{i=1}^{|T_B|}\ell_{\mathrm{OE}}(\mathbf{h}(\mathbf{g}(\mathbf{x}_A^i) + \mathbf{p}^i)) + \alpha\frac{1}{|S_B|}\sum_{i=1}^{|S_B|}\ell(\mathbf{f}_\mathbf{w}; \mathbf{x}_I^i, y_I^i))\right]$;

end for

Output: model parameter $\mathbf{w}$.

Furthermore, under proper conditions, one can show that the bound in Eq. (11) can attain $\mathcal{O}(1/\sqrt{n}) + \mathcal{O}(1/\sqrt{m})$, i.e., $R_D(\widehat{\mathbf{w}}; \rho) - \min_{\mathbf{w} \in \mathcal{W}} R_D(\mathbf{w}; \rho) \leq \mathcal{O}(1/\sqrt{n}) + \mathcal{O}(1/\sqrt{m})$. Corollary 1 in Appendix C.5 gives an example to support the above claim. Next, we give a learning bound to estimate the expected detection risk in Eq. (2) w.r.t. the model $\mathbf{f}_{\widehat{\mathbf{w}}}$ given by Eq. (8).

Theorem 3 (Risk Estimation). *Given the same conditions in Theorem 2 and let $\widehat{\mathbf{w}}$ be the solution of Eq. (8), which is given by $\widehat{\mathbf{w}} \in \arg\min_{\mathbf{w} \in \mathcal{W}} \widehat{R}_D(\mathbf{w}; \rho)$. If $\ell_{\mathrm{OE}}(\mathbf{f}_\mathbf{w}; \mathbf{x})$ is L_c-Lipschitz w.r.t. $c(\cdot, \cdot)$, i.e., $|\ell_{\mathrm{OE}}(\mathbf{f}_\mathbf{w}; \mathbf{x}) - \ell_{\mathrm{OE}}(\mathbf{f}_\mathbf{w}; \mathbf{x}')| \leq L_c c(\mathbf{x}, \mathbf{x}')$, then with the probability at least $1 - 4e^{-t} > 0$,*

$$R_D(\widehat{\mathbf{w}}) - \overbrace{\min_{\mathbf{w} \in \mathcal{W}} R_D(\mathbf{w}; \rho)}^{\text{approximate risk}} \leq \underbrace{\alpha L_c \max\{\mathrm{W}_c(D_{X_O}, D_{X_A}) - \rho, 0\} + \epsilon(n, m; t)}_{\text{estimation error}},$$

for any $\rho > 0$, where $\epsilon(n, m; t)$ is defined in Theorem 2.

The bias term $\alpha L_c \max\{\mathrm{W}_c(D_{X_O}, D_{X_A}) - \rho, 0\} = 0$ when ρ is large enough. Hence, a large ρ implies a small estimation error. Although a larger ρ leads to better generalization ability, the approximate risk $\min_{\mathbf{w} \in \mathcal{W}} R_D(\mathbf{w}; \rho)$ may become larger. It implies that for practical effectiveness, i.e., small $R_D(\widehat{\mathbf{w}})$, there is a trade-off between the approximate risk $\min_{\mathbf{w} \in \mathcal{W}} R_D(\mathbf{w}; \rho)$ and the bias $\alpha L_c \max\{\mathrm{W}_c(D_{X_O}, D_{X_A}) - \rho, 0\}$ across different choices of ρ. Hence, we need to choose a proper ρ for open-world detection with unseen data (cf., Section 5.3).

4.2 Proposed Algorithm

In this section, we introduce the algorithm design for DAL, summarized in Algorithm 1. Due to the space limit, we provide further discussions in Appendix E.

Losses and Cost Function. Following Hendrycks et al. (2019), we adopt the cross entropy loss to realize ℓ and the KL-divergence between model predictions and uniform distribution for ℓ_{OE}. We also define the cost function c by the l_1 norm, namely, $c(\mathbf{x}, \mathbf{x}') = \|\mathbf{x} - \mathbf{x}'\|_1$.

Algorithm Design. By Theorem 1, we can address the primary problem in Eq. (8) by the dual problem in Eq. (9). Additionally, following Du et al. (2022a), we perturb for the worst OOD data in the embedding space. Denote the model $\mathbf{f}_\mathbf{w} = \mathbf{h} \circ \mathbf{e}$ with $\mathbf{h}$ the classifier and $\mathbf{e}$ the feature extractor, we find the perturbation $\mathbf{p}$ for the embedding features, i.e., $\mathbf{e}(\mathbf{x})$, of the associated data $\mathbf{x}$. The perturbation $\mathbf{p}$ should lead to the worst OOD case for the surrogate function in Theorem 1, namely,

$$\phi_\gamma(\mathbf{w}; \mathbf{e}(\mathbf{x})) = \sup_{\mathbf{p} \in \mathcal{E}} \{\ell_{\mathrm{OE}}(\mathbf{h}(\mathbf{e}(\mathbf{x}) + \mathbf{p}); \mathbf{e}(\mathbf{x})) - \gamma\|\mathbf{p}\|_1\},$$

where $\mathcal{E}$ denotes the space of embedding features. Note that we abuse the definition of ℓ_{OE}, emphasizing that we perturb the embedding features of $\mathbf{e}(\mathbf{x})$ by $\mathbf{p}$.

Training and Inference. Our definition of $\phi_\gamma(\mathbf{w}; \mathbf{e}(\mathbf{x}))$ leads to a particular realization of Eq. (10), which is the learning objective of our DAL. It can be solved by stochastic gradient optimization for deep models, e.g., mini-batch stochastic gradient descent. After training, we use the MSP scoring function by default and discuss the possibility of other scoring functions in Appendix F.3.

Stochastic Realization. Algorithm 1 gives a stochastic realization of DAL, where ID and auxiliary OOD mini-batches are randomly sampled in each stochastic iteration, denoted by S_B and T_B respectively. Therein, we first find the perturbation $\mathbf{p}$ that leads to the maximal $\phi_\gamma(\mathbf{w}, \mathbf{e}(\mathbf{x}))$. The value of $\mathbf{p}$ is initialized by random Gaussian noise with the standard deviation σ and updated by gradient ascent for `num_search` steps with the perturbation strength `ps`. Then we update γ by one step of gradient descent with the learning rate β, and further clipping between 0 and γ_{max} to avoid extreme values. Finally, given the proper perturbations for the auxiliary OOD data in T_B, we update the model parameter $\mathbf{w}$ by one step of mini-batch gradient descent.

5 Experiments

In this section, we mainly test DAL on the CIFAR (Krizhevsky and Hinton, 2009) benchmarks (as ID datasets). To begin with, we introduce the evaluation setups.

OOD Datasets. We adopt the 80 Million Tiny Images (Torralba et al., 2008) as the auxiliary OOD dataset; Textures (Cimpoi et al., 2014), SVHN (Netzer et al., 2011), Places365 (Zhou et al., 2018), LSUN (Yu et al., 2015), and iSUN (Xu et al., 2015) as the (test-time) real OOD datasets. We eliminate those data whose labels coincide with ID cases.

Pre-training Setups. We employ Wide ResNet-40-2 (Zagoruyko and Komodakis, 2016) trained for 200 epochs via empirical risk minimization, with a batch size 64, momentum 0.9, and initial learning rate 0.1. The learning rate is divided by 10 after 100 and 150 epochs.

Hyper-parameters Tuning Strategy. The hyper-parameters are tuned based on the validation data, separated from the training ID and auxiliary OOD data, which is a common strategy in OOD detection with outlier exposure field (Hendrycks et al., 2019; Chen et al., 2021). Specifically, we fix $\sigma = 0.001$, `num_search` $= 10$, and adopt the grid search to choose γ_{max} from $\{0.1, 0.5, 1, 5, 10, 50\}$; β from $\{1e^{-3}, 5e^{-3}, 1e^{-2}, 5e^{-2}, 1e^{-1}, 5e^{-1}, 1, 5\}$; ρ from $\{1e^{-2}, 1e^{-1}, 1, 10, 100\}$; `ps` from $\{1e^{-3}, 1e^{-2}, 1e^{-1}, 1, 10, 100\}$; α from $\{0.1, 0.5, 1.0, 1.5, 2.0\}$.

Hyper-parameters Setups. For CIFAR-10, DAL is run for 50 epochs with the ID batch size 128, the OOD batch size 256, the initial learning rate 0.07, $\gamma_{max} = 10$, $\beta = 0.01$, $\rho = 10$, `ps` $= 1$, and $\alpha = 1$. For CIFAR-100, DAL is run for 50 epochs with the ID batch size 128, the OOD batch size 256, the initial learning rate 0.07, $\gamma_{max} = 10$, $\beta = 0.005$, $\rho = 10$, and `ps` $= 1$, and $\alpha = 1$. For both cases, we employ cosine decay (Loshchilov and Hutter, 2017) for the model learning rate.

Baseline Methods. We compare DAL with representative methods, including MSP (Hendrycks and Gimpel, 2017), Free Energy (Liu et al., 2020), ASH (Djurisic et al., 2023), ReAct (Sun et al., 2021), Mahalanobis (Lee et al., 2018a), KNN (Sun et al., 2022), KNN+ (Sun et al., 2022), CSI (Tack et al., 2020), VOS (Du et al., 2022a), Outlier Exposure (OE) (Hendrycks et al., 2019), Energy-OE (Liu et al., 2020), ATOM (Chen et al., 2021), DOE (Wang et al., 2023), and POEM (Ming et al., 2022). We adopt their suggested setups but unify the backbones for fairness.

Evaluation Metrics. The detection performance is evaluated via two representative metrics, which are both threshold-independent: the false positive rate of OOD data when the true positive rate of ID data is at 95% (FPR95); and the area under the receiver operating characteristic curve (AUROC), which can be viewed as the probability of the ID case having greater score than that of the OOD case.

Due to the space limit, we test our DAL with more advanced scoring strategies in Appendix F.3 and conduct experiments on the more complex ImageNet (Deng et al., 2009) dataset in Appendix F.10.

5.1 Main Results

The main results are summarized in Table 1, where we report the detailed results across the considered real OOD datasets. First, we reveal that using auxiliary OOD data can generally lead to better results than using only ID information, indicating that outlier exposure remains a promising direction worth studying. However, as demonstrated in Section 3, the OOD distribution discrepancy can hurt its open-world detection power, while previous works typically oversee such an important issue. Therefore, our DAL, which can alleviate the OOD distribution discrepancy, reveals a large improvement over the original outlier exposure. Specifically, comparing with the conventional outlier exposure, our method reveals 1.99 and 0.13 average improvements w.r.t. FPR95 and AUROC on the CIFAR-10 dataset, and 13.46 and 3.65 of the average improvements on CIFAR-100 dataset. For advanced works that consider the OOD sampling strategies, e.g., ATOM and POEM, DAL can achieve much better results, especially for the CIFAR-100 case. The reason is that these methods mainly consider the situations

Table 1: Comparison between our method and advanced methods on the CIFAR benchmarks. ↓ (or ↑) indicates smaller (or larger) values are preferred, and a bold font indicates the best result in a column. Methods are grouped based on 1) using ID data only and 2) using additional information about auxiliary OOD data. Two groups are separated by the horizontal line for each ID case.

Method	SVHN		LSUN		iSUN		Textures		Places365		Average	
	FPR95↓	AUROC↑	FPR95↓	AUROC↑	FPR95↓	AUROC↑	FPR95↓	AUROC↑	FPR95↓	AUROC↑	FPR95↓	AUROC↑
CIFAR-10												
Using ID data only												
MSP	48.89	91.97	25.53	96.49	56.44	89.86	59.68	88.42	60.19	88.36	50.15	91.02
Free Energy	35.21	91.24	4.42	99.06	33.84	92.56	52.46	85.35	40.11	90.02	33.21	91.64
ASH	33.98	91.79	4.76	98.98	34.38	92.64	50.90	86.07	40.89	89.79	32.98	91.85
Mahalanobis	12.21	97.70	57.25	89.58	79.74	77.87	15.20	95.40	68.81	82.39	46.64	88.59
KNN	26.56	95.93	27.52	95.43	33.55	93.15	37.62	93.07	41.67	91.21	33.38	93.76
KNN+	3.28	99.33	2.24	98.90	17.85	95.65	10.87	97.72	30.63	94.98	12.97	97.32
CSI	17.37	97.69	6.75	98.46	12.58	97.95	25.65	94.70	40.00	92.05	20.47	96.17
VOS	36.55	93.30	9.98	98.03	28.93	94.25	52.83	85.74	39.56	89.71	33.57	92.21
Using ID data and auxiliary OOD data												
OE	2.36	99.27	1.15	**99.68**	2.48	99.34	5.35	98.88	11.99	97.23	4.67	98.88
Energy-OE	0.97	99.54	1.00	99.15	2.32	99.27	3.42	**99.18**	9.57	97.44	3.46	98.91
ATOM	1.00	99.59	0.61	99.53	2.15	**99.40**	2.52	99.10	7.93	97.27	2.84	98.97
DOE	1.80	99.37	**0.25**	99.65	2.00	99.36	5.65	98.75	10.15	97.28	3.97	98.88
POEM	1.20	99.53	0.80	99.10	**1.47**	99.26	2.93	99.13	7.65	97.35	2.81	98.87
DAL	**0.80**	**99.65**	0.90	99.46	1.70	99.34	**2.30**	99.14	**7.65**	**97.45**	**2.68**	**99.01**
CIFAR-100												
Using ID data only												
MSP	84.39	71.18	60.36	85.59	82.63	75.69	83.32	73.59	82.37	73.69	78.61	75.95
Free Energy	85.24	73.71	23.05	95.89	81.11	79.02	79.63	76.35	80.18	75.65	69.84	80.12
ASH	70.09	83.56	13.20	97.71	69.87	82.56	63.69	83.59	79.70	74.87	59.31	84.46
Mahalanobis	51.00	88.70	91.60	69.69	38.48	91.86	47.07	89.09	82.70	74.18	72.37	82.70
KNN	52.10	88.83	68.82	79.00	42.17	90.59	42.79	89.07	92.21	61.08	59.62	81.71
KNN+	32.50	93.86	47.41	84.93	39.82	91.12	43.05	88.55	63.26	79.28	45.20	87.55
CSI	64.50	84.62	25.88	95.93	70.62	80.83	61.50	86.74	83.08	77.11	61.12	95.05
VOS	78.06	92.59	40.40	92.90	85.77	70.20	82.46	77.22	82.31	75.47	73.80	91.67
Using ID data and auxiliary OOD data												
OE	46.73	90.54	16.30	96.98	47.97	88.43	50.39	88.27	54.30	87.11	43.14	90.27
Energy-OE	35.34	94.74	16.27	97.25	33.21	93.25	46.13	90.62	50.45	90.04	36.28	93.18
ATOM	24.80	95.15	17.83	96.76	47.83	91.06	44.86	**91.80**	53.92	88.88	37.84	92.73
DOE	43.10	91.83	13.95	**97.56**	47.25	87.88	49.40	88.62	51.05	88.08	40.95	90.79
POEM	22.27	**96.28**	**13.66**	97.52	42.46	91.97	45.94	90.42	49.50	90.21	34.77	93.28
DAL	**19.35**	96.21	16.05	96.78	**26.05**	**94.23**	**37.60**	91.57	**49.35**	**90.81**	**29.68**	**93.92**

where the model capacity is not enough to learn from all the auxiliary OOD data, deviating from our considered issue in OOD distribution discrepancy. Moreover, for the previous works that adopt similar concepts in the worst-case OOD learning, e.g., VOS and DOE, DAL also reveals better results, with 1.29 and 30.89 improvements on the CIFAR-10 dataset and 11.27 and 44.12 improvements on the CIFAR-100 dataset w.r.t. FPR95. It indicates that our theoretical-driven scheme can also guide the algorithm designs with practical effectiveness. Note that many previous works use advanced scoring strategies other than MSP, and thus our experiment above is not completely fair to us. Therefore, in Appendix F.3, we also combine DAL with many advanced scoring strategies other than MSP, which can further improve our performance.

5.2 Hard OOD Detection

We further consider hard OOD scenarios (Sun et al., 2022), of which the test OOD data are very similar to that of the ID cases. Following the common setup (Sun et al., 2022) with the CIFAR-10 dataset being the ID case, we evaluate our DAL on three hard OOD datasets, namely, LSUN-Fix (Yu et al., 2015), ImageNet-Resize (Deng et al., 2009), and CIFAR-100. Note that data in ImageNet-Resize (1000 classes) with the same semantic space as Tiny-ImageNet (200 classes) are removed. We select a set of strong baselines that

Table 2: Comparison between our method and advanced methods on hard OOD detection. ↓ (or ↑) indicates smaller (or larger) values are preferred, and a bold font indicates the best result in a column.

Methods	LSUN-Fix		ImageNet-Resize		CIFAR-100	
	FPR95↓	AUROC↑	FPR95↓	AUROC↑	FPR95↓	AUROC↑
Using ID data only						
Free Energy	6.42	98.85	46.46	89.02	50.47	87.08
ASH	4.00	98.20	46.18	88.85	54.31	83.71
KNN+	24.88	95.75	30.52	94.85	40.00	89.11
CSI	39.79	93.63	37.47	93.93	45.64	87.64
Using ID data and auxiliary OOD data						
OE	1.75	99.47	6.76	98.58	29.40	94.20
DOE	1.97	98.71	5.98	98.75	29.75	94.24
POEM	**1.24**	98.93	6.56	98.37	35.11	91.80
DAL	1.39	**99.47**	**5.60**	**98.80**	**25.45**	**94.34**

are competent in hard OOD detection, summarizing the experiments in Table 2. As we can see, our method can beat these advanced methods across the considered datasets, even for the challenging
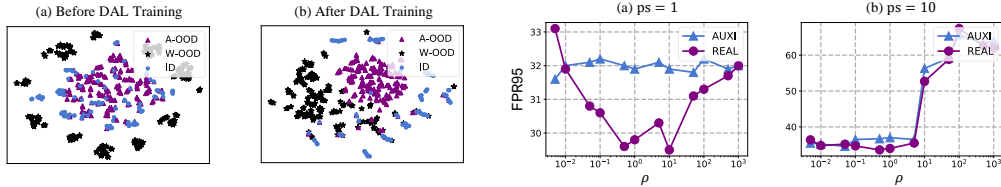
Figure 2: Illustrations of embedding features for the ID, the auxiliary OOD (A-OOD), and the worst OOD (W-OOD) data. We adopt the t-SNE visualization on the CIFAR-10 dataset and illustrate the results before and after DAL training.

Figure 3: FPR95 curves across various ρ on the CIFAR-100. We report both the results for the average real OOD data (REAL) and the auxiliary OOD data (AUXI), where we consider two hyperparameter setups, i.e., $\mathtt{ps} = 1$ and $\mathtt{ps} = 10$.

CIFAR-10 versus CIFAR-100 setting. The reason is that our distributional augmentation directly learns from OOD data close to ID pattern, which can cover hard OOD cases.

5.3 Ablation Study

We further conduct an ablation study to demonstrate two mechanisms that mainly contribute to our open-world effectiveness, namely, OOD data generation and Wasserstein ball constraint.

OOD Data Generation. DAL learns from the worst OOD data to mitigate the OOD distribution discrepancy. To understand such an OOD generation scheme, we employ the t-SNE visualization (Van der Maaten and Hinton, 2008) for the ID, the auxiliary OOD, and the worst OOD data. Figure 2 summarizes the results before and after DAL training. Before training, the ID and auxiliary OOD data overlap largely, indicating that the original model is not effective at distinguishing between them. Then, DAL does not directly train the model on auxiliary OOD data but instead perturbs it to further confuse the model beyond the overlap region. After DAL training, the overlap region between ID and auxiliary OOD data shrinks. Additionally, perturbing the original OOD data becomes more difficult, indicating that the model has learned to handle various worst-case OOD scenarios.

Wasserstein Ball Constraint. The choice of ρ determines the radius of the Wasserstein ball. Larger values of ρ reduce estimation error and improve model generalization, as stated in Theorem 3. However, larger values of ρ also increase the approximate risk $\min_{\mathbf{w} \in \mathcal{W}} R_D(\mathbf{w}; \rho)$ as it becomes more challenging to ensure uniform model performance with increased distributional perturbation. Figure 3 shows the FPR95 curves on the CIFAR-100 dataset for both the real and the surrogate OOD data, revealing the trade-off in selecting ρ. Here, we consider two setups of ρ, i.e., $\mathtt{ps} = 1$ (default) and $\mathtt{ps} = 10$ (large perturbation strength). First, when the perturbation strength is very large (i.e., $\mathtt{ps} = 10$), the model can easily fail for training if the value of ρ is also large (e.g., $\rho = 100$), indicating that large value of ρ can lead to a large approximation error. However, such an issue can be overcome by selecting a relatively small value of ρ (e.g., $\rho = 0.5$).

6   Conclusion

Outlier exposure is one of the most powerful methods in OOD detection, but the discrepancy between the auxiliary and (unseen) real OOD data can hinder its practical effectiveness. To address such an issue, we have formalized it as the OOD distribution discrepancy and developed an effective learning framework to mitigate its negative impacts. Specifically, we consider a specific distribution set that contains all distributions in a Wasserstein ball centered on the auxiliary OOD distribution. Then, models trained over worst-case OOD data in the ball can ensure improved performance toward open-world OOD detection. Overall, as pioneers in critically analyzing the open-world setting with theoretical analysis, we are committed to raising attention to the OOD distribution discrepancy issue and encouraging further research in this direction.

Acknowledgments and Disclosure of Funding

References

Dan Hendrycks and Kevin Gimpel. A baseline for detecting misclassified and out-of-distribution examples in neural networks. In *ICLR*, 2017.

Zhen Fang, Yixuan Li, Jie Lu, Jiahua Dong, Bo Han, and Feng Liu. Is out-of-distribution detection learnable? In *NeurIPS*, 2022.

Saikiran Bulusu, Bhavya Kailkhura, Bo Li, P Varshney, and Dawn Song. Anomalous instance detection in deep learning: A survey. Technical report, Lawrence Livermore National Lab., 2020.

Jingkang Yang, Kaiyang Zhou, Yixuan Li, and Ziwei Liu. Generalized out-of-distribution detection: a survey. *arXiv preprint arXiv:2110.11334*, 2021.

Tianshi Cao, Chin-Wei Huang, David Yu-Tung Hui, and Joseph Paul Cohen. A benchmark of medical out of distribution detection. *arXiv preprint arXiv:2007.04250*, 2020.

Zheyan Shen, Jiashuo Liu, Yue He, Xingxuan Zhang, Renzhe Xu, Han Yu, and Peng Cui. Towards out-of-distribution generalization: A survey. *arXiv preprint arXiv:2108.13624*, 2021.

Dan Hendrycks, Mantas Mazeika, and Thomas G. Dietterich. Deep anomaly detection with outlier exposure. In *ICLR*, 2019.

Yifei Ming, Ying Fan, and Yixuan Li. POEM: Out-of-distribution detection with posterior sampling. In *ICML*, 2022.

Qizhou Wang, Junjie Ye, Feng Liu, Quanyu Dai, Marcus Kalander, Tongliang Liu, Jianye Hao, and Bo Han. Out-of-distribution detection with implicit outlier transformation. In *ICLR*, 2023.

Cédric Villani. *Topics in Optimal Transportation*. American Mathematical Society, 2021.

Cédric Villani. *Optimal Transport: Old and New*. Springer, 2008.

Xuefeng Du, Zhaoning Wang, Mu Cai, and Yixuan Li. VOS: Learning what you don't know by virtual outlier synthesis. In *ICLR*, 2022a.

Akshay Mehra, Bhavya Kailkhura, Pin-Yu Chen, and Jihun Hamm. On certifying and improving generalization to unseen domains. *arXiv preprint arXiv:2206.12364*, 2022.

Jiefeng Chen, Yixuan Li, Xi Wu, Yingyu Liang, and Somesh Jha. ATOM: Robustifying out-of-distribution detection using outlier mining. In *ECML*, 2021.

Kimin Lee, Kibok Lee, Honglak Lee, and Jinwoo Shin. A simple unified framework for detecting out-of-distribution samples and adversarial attacks. In *NeurIPS*, 2018a.

Weitang Liu, Xiaoyun Wang, John D Owens, and Yixuan Li. Energy-based out-of-distribution detection. In *NeurIPS*, 2020.

Yiyou Sun, Yifei Ming, Xiaojin Zhu, and Yixuan Li. Out-of-distribution detection with deep nearest neighbors. In *ICML*, 2022.

Aman Sinha, Hongseok Namkoong, and John C. Duchi. Certifying some distributional robustness with principled adversarial training. In *ICLR*, 2018.

Hongseok Namkoong and John C. Duchi. Stochastic gradient methods for distributionally robust optimization with f-divergences. In *NIPS*, 2016.

Paul Michel, Tatsunori Hashimoto, and Graham Neubig. Modeling the second player in distributionally robust optimization. In *ICLR*, 2021.

Matthew Staib and Stefanie Jegelka. Distributionally robust optimization and generalization in kernel methods. In *NeurIPS*, 2019.

Rui Dai, Yonggang Zhang, Zhen Fang, Bo Han, and Xinmei Tian. Moderately distributional exploration for domain generalization. In *ICML*, 2023.

José H. Blanchet and M. KarthyekRajhaaA. Quantifying distributional model risk via optimal transport. *Risk Management eJournal*, 2016.

Alex Krizhevsky and Geoffrey Hinton. Learning multiple layers of features from tiny images. *Technical Report TR-2009, University of Toronto*, 2009.

Antonio Torralba, Rob Fergus, and William T Freeman. 80 million tiny images: A large data set for nonparametric object and scene recognition. *IEEE transactions on pattern analysis and machine intelligence*, 30(11):1958–1970, 2008.

Mircea Cimpoi, Subhransu Maji, Iasonas Kokkinos, Sammy Mohamed, and Andrea Vedaldi. Describing textures in the wild. In *CVPR*, 2014.

Yuval Netzer, Tao Wang, Adam Coates, Alessandro Bissacco, Bo Wu, and Andrew Y Ng. Reading digits in natural images with unsupervised feature learning. In *NIPS Workshop*, 2011.

Bolei Zhou, Àgata Lapedriza, Aditya Khosla, Aude Oliva, and Antonio Torralba. Places: A 10 million image database for scene recognition. *IEEE Transactions on Pattern Analysis and Machine Intelligence*, 40(6):1452–1464, 2018.

Fisher Yu, Ari Seff, Yinda Zhang, Shuran Song, Thomas Funkhouser, and Jianxiong Xiao. LSUN: construction of a large-scale image dataset using deep learning with humans in the loop. *arXiv preprint arXiv:1506.03365*, 2015.

Pingmei Xu, Krista A Ehinger, Yinda Zhang, Adam Finkelstein, Sanjeev R Kulkarni, and Jianxiong Xiao. Turkergaze: crowdsourcing saliency with webcam based eye tracking. *arXiv preprint arXiv:1504.06755*, 2015.

Sergey Zagoruyko and Nikos Komodakis. Wide residual networks. In *BMVC*, 2016.

Ilya Loshchilov and Frank Hutter. SGDR: Stochastic gradient descent with warm restarts. In *ICLR*, 2017.

Andrija Djurisic, Nebojsa Bozanic, Arjun Ashok, and Rosanne Liu. Extremely simple activation shaping for out-of-distribution detection. In *ICLR*, 2023.

Yiyou Sun, Chuan Guo, and Yixuan Li. ReAct: out-of-distribution detection with rectified activations. In *NeurIPS*, 2021.

Jihoon Tack, Sangwoo Mo, Jongheon Jeong, and Jinwoo Shin. CSI: novelty detection via contrastive learning on distributionally shifted instances. In *NeurIPS*, 2020.

Jia Deng, Wei Dong, Richard Socher, Li-Jia Li, Kai Li, and Li Fei-Fei. ImageNet: a large-scale hierarchical image database. In *CVPR*, 2009.

Laurens Van der Maaten and Geoffrey Hinton. Visualizing data using t-SNE. *Journal of machine learning research*, 9(11):2579–2605, 2008.

Shiyu Liang, Yixuan Li, and R. Srikant. Enhancing the reliability of out-of-distribution image detection in neural networks. In *ICLR*, 2018.

Haoran Wang, Weitang Liu, Alex Bocchieri, and Yixuan Li. Can multi-label classification networks know what they don't know? In *NeurIPS*, 2021a.

Balaji Lakshminarayanan, Alexander Pritzel, and Charles Blundell. Simple and scalable predictive uncertainty estimation using deep ensembles. In *NIPS*, 2017.

Rui Huang and Yixuan Li. MOS: towards scaling out-of-distribution detection for large semantic space. In *CVPR*, 2021.

Chandramouli Shama Sastry and Sageev Oore. Detecting out-of-distribution examples with gram matrices. In *ICML*, 2020.

Haoqi Wang, Zhizhong Li, Litong Feng, and Wayne Zhang. ViM: Out-of-distribution with virtual-logit matching. In *CVPR*, 2022a.

Ziqian Lin, Sreya Dutta Roy, and Yixuan Li. MOOD: Multi-level out-of-distribution detection. In *CVPR*, 2021.

Peyman Morteza and Yixuan Li. Provable guarantees for understanding out-of-distribution detection. In *AAAI*, 2022.

Yadan Luo, Zijian Wang, Zhuoxiao Chen, Zi Huang, and Mahsa Baktashmotlagh. Source-free progressive graph learning for open-set domain adaptation. *IEEE Transactions on Pattern Analysis and Machine Intelligence*, 45(9):11240–11255, 2023.

Rui Huang, Andrew Geng, and Yixuan Li. On the importance of gradients for detecting distributional shifts in the wild. In *NeurIPS*, 2021.

Conor Igoe, Youngseog Chung, Ian Char, and Jeff Schneider. How useful are gradients for ood detection really? *arXiv preprint arXiv:2205.10439*, 2022.

Jianing Zhu, Hengzhuang Li, Jiangchao Yao, Tongliang Liu, Jianliang Xu, and Bo Han. Unleashing mask: Explore the intrinsic out-of-distribution detection capability. In *ICML*, 2023a.

Vikash Sehwag, Mung Chiang, and Prateek Mittal. SSD: A unified framework for self-supervised outlier detection. In *ICLR*, 2021.

Haotao Wang, Aston Zhang, Yi Zhu, Shuai Zheng, Mu Li, Alex J Smola, and Zhangyang Wang. Partial and asymmetric contrastive learning for out-of-distribution detection in long-tailed recognition. In *ICML*, 2022b.

Haotian Zheng, Qizhou Wang, Zhen Fang, Xiaobo Xia, Feng Liu, Tongliang Liu, and Bo Han. Out-of-distribution detection learning with unreliable out-of-distribution sources. In *NeurIPS*, 2023.

Xuefeng Du, Gabriel Gozum, Yifei Ming, and Yixuan Li. SIREN: Shaping representations for detecting out-of-distribution objects. In *NeurIPS*, 2022b.

Yifei Ming, Yiyou Sun, Ousmane Dia, and Yixuan Li. How to exploit hyperspherical embeddings for out-of-distribution detection? In *ICLR*, 2023.

Alireza Zaeemzadeh, Niccolò Bisagno, Zeno Sambugaro, Nicola Conci, Nazanin Rahnavard, and Mubarak Shah. Out-of-distribution detection using union of 1-dimensional subspaces. In *CVPR*, 2021.

Hongxin Wei, Renchunzi Xie, Hao Cheng, Lei Feng, Bo An, and Yixuan Li. Mitigating neural network overconfidence with logit normalization. In *ICML*, 2022.

Zhuo Huang, Xiaobo Xia, Li Shen, Bo Han, Mingming Gong, Chen Gong, and Tongliang Liu. Harnessing out-of-distribution examples via augmenting content and style. In *ICLR*, 2023a.

Jianing Zhu, Geng Yu, Jiangchao Yao, Tongliang Liu, Gang Niu, Masashi Sugiyama, and Bo Han. Diversified outlier exposure for out-of-distribution detection via informative extrapolation. In *NeurIPS*, 2023b.

Yi Li and Nuno Vasconcelos. Background data resampling for outlier-aware classification. In *CVPR*, 2020.

Matthias Hein, Maksym Andriushchenko, and Julian Bitterwolf. Why relu networks yield high-confidence predictions far away from the training data and how to mitigate the problem. In *CVPR*, 2019.

Taewon Jeong and Heeyoung Kim. OOD-MAMl: Meta-learning for few-shot out-of-distribution detection and classification. In *NeurIPS*, 2020.

Joost Van Amersfoort, Lewis Smith, Yee Whye Teh, and Yarin Gal. Uncertainty estimation using a single deep deterministic neural network. In *ICML*, 2020.

Kimin Lee, Honglak Lee, Kibok Lee, and Jinwoo Shin. Training confidence-calibrated classifiers for detecting out-of-distribution samples. In *ICLR*, 2018b.

Sachin Vernekar, Ashish Gaurav, Vahdat Abdelzad, Taylor Denouden, Rick Salay, and Krzysztof Czarnecki. Out-of-distribution detection in classifiers via generation. In *NeurIPS Workshop*, 2019.

Leitian Tao, Xuefeng Du, Xiaojin Zhu, and Yixuan Li. Non-parametric outlier synthesis. In *ICLR*, 2023.

Yadan Luo, Zijian Wang, Zi Huang, and Mahsa Baktashmotlagh. Progressive graph learning for open-set domain adaptation. In *ICML*, 2020.

Lily H. Zhang, Mark Goldstein, and Rajesh Ranganath. Understanding failures in out-of-distribution detection with deep generative models. In *ICML*, 2021.

Zhen Fang, Jie Lu, Anjin Liu, Feng Liu, and Guangquan Zhang. Learning bounds for open-set learning. In *ICML*, 2021.

Julian Bitterwolf, Alexander Meinke, Maximilian Augustin, and Matthias Hein. Breaking down out-of-distribution detection: Many methods based on OOD training data estimate a combination of the same core quantities. In *ICML*, 2022.

Roman Vershynin. *High-Dimensional Probability*. Springer, 2018.

Jose Blanchet, Yang Kang, and Karthyek Murthy. Robust wasserstein profile inference and applications to machine learning. *Journal of Applied Probability*, 56(3):830–857, 2019.

Noah Golowich, Alexander Rakhlin, and Ohad Shamir. Size-independent sample complexity of neural networks. In *COLT*, 2018.

Aleksander Madry, Aleksandar Makelov, Ludwig Schmidt, Dimitris Tsipras, and Adrian Vladu. Towards deep learning models resistant to adversarial attacks. In *ICLR*, 2018.

Qizhou Wang, Feng Liu, Bo Han, Tongliang Liu, Chen Gong, Gang Niu, Mingyuan Zhou, and Masashi Sugiyama. Probabilistic margins for instance reweighting in adversarial training. In *NeurIPS*, 2021b.

Zhuo Huang, Miaoxi Zhu, Xiaobo Xia, Li Shen, Jun Yu, Chen Gong, Bo Han, Bo Du, and Tongliang Liu. Robust generalization against photon-limited corruptions via worst-case sharpness minimization. In *CVPR*, 2023b.

Risheng Liu, Jiaxin Gao, Jin Zhang, Deyu Meng, and Zhouchen Lin. Investigating bi-level optimization for learning and vision from a unified perspective: A survey and beyond. *IEEE Transactions on Pattern Analysis and Machine Intelligence*, 44(12):10045–10067, 2021.

Yonggang Zhang, Mingming Gong, Tongliang Liu, Gang Niu, Xinmei Tian, Bo Han, Bernhard Schölkopf, and Kun Zhang. Adversarial robustness through the lens of causality. In *ICLR*, 2022.

Tal Ridnik, Emanuel Ben-Baruch, Asaf Noy, and Lihi Zelnik-Manor. ImageNet-21k pretraining for the masses. *arXiv preprint arXiv:2104.10972*, 2021.

Grant Van Horn, Oisin Mac Aodha, Yang Song, Yin Cui, Chen Sun, Alexander Shepard, Hartwig Adam, Pietro Perona, and Serge J. Belongie. The iNaturalist species classification and detection dataset. In *CVPR*, 2018.

Dan Hendrycks, Steven Basart, Mantas Mazeika, Mohammadreza Mostajabi, Jacob Steinhardt, and Dawn Song. Scaling out-of-distribution detection for real-world settings. In *ICML*, 2022.

A Related Works

In this section, we discuss the related studies in OOD detection.

OOD Detection Methods. Existing works in OOD detection can be mainly categorized into three categories, namely, the post-hoc methods, the representation-based methods, and the outlier exposure. For the post-hoc methods, they believe a well-trained ID classifier can already lead to effective OOD detection (Hendrycks and Gimpel, 2017), given proper scoring functions to indicate ID and OOD cases. Existing scoring functions are built upon the classifiers, taking logit outputs (Hendrycks and Gimpel, 2017; Liang et al., 2018; Liu et al., 2020; Sun et al., 2021; Wang et al., 2021a; Lakshminarayanan et al., 2017; Wang et al., 2021a; Huang and Li, 2021), embedding features (Lee et al., 2018a; Sastry and Oore, 2020; Wang et al., 2022a; Lin et al., 2021; Sun et al., 2022; Morteza and Li, 2022; Luo et al., 2023), or gradient information (Huang et al., 2021; Liang et al., 2018; Igoe et al., 2022) as its inputs and returning a score value to indicate the confidence for an ID case. Recent works focus on adaptation strategies for specific tasks (Huang et al., 2021; Zhu et al., 2023a) and non-parametric approaches (Sun et al., 2022), which may motivate future works.

Other works believe that training procedures are indispensable in OOD detection. For representation-based methods, researchers assume that a good ID representation is all we need for effective OOD detection. Therein, researchers study contrastive learning methods (Sehwag et al., 2021; Wang et al., 2022b), data augmentation (Tack et al., 2020; Zheng et al., 2023), constraints on embedding features (Du et al., 2022b; Ming et al., 2023; Zaeemzadeh et al., 2021) or model output (Wei et al., 2022). However, some of the adopted scoring functions in representation-based methods are complex. It can make us overestimate the true effects of representation learning, which may require further studies. For outlier exposure, related methods directly make the model learn from OOD data with low OOD score predictions (Hendrycks et al., 2019; Liu et al., 2020; Huang et al., 2023a). Related works studies sampling strategies (Zhu et al., 2023b; Ming et al., 2022; Chen et al., 2021), adversarial robust learning (Li and Vasconcelos, 2020; Lee et al., 2018a; Hein et al., 2019), meta learning (Jeong and Kim, 2020), and regularization strategies (Van Amersfoort et al., 2020). Other works consider the situations where OOD data are inaccessible, studying various outlier synthesis strategies (Lee et al., 2018b; Vernekar et al., 2019; Du et al., 2022a; Tao et al., 2023). Although outlier exposure typically reveals promising results, the difference between auxiliary and real OOD data largely hinders its real-world detection power, similar to conclusions in domain adaptation (Luo et al., 2023, 2020).

OOD Detection Theory. Zhang et al. (2021) gives an explanation of why there exist OOD data that have higher probabilities or densities than the data from the ID distribution in the deep generative models. Zhang et al. (2021) understands OOD detection via goodness-of-fit tests and points out that OOD detection should be defined based on the data distribution's typical set if we hope OOD detection can be successful. Morteza and Li (2022) develops a novel unified framework that helps researchers to understand the theoretical connections among some representative OOD detection methods. Fang et al. (2021, 2022) develop the probably approximately correct (PAC) learning theory for OOD detection and gives a series of sufficient and necessary conditions for the PAC learnability of OOD detection. Fang et al. (2022) has proven that although OOD detection cannot be PAC learnable in the distribution-free case, OOD detection can be successful in many practical scenarios. Note that Zhang et al. (2021), Morteza and Li (2022), and Fang et al. (2022) all consider the case that the auxiliary OOD data are unavailable. Therefore, to ensure the leanability of OOD detection, some strong conditions are necessary (Zhang et al., 2021; Fang et al., 2022). To explore the outlier exposure case in OOD detection, Bitterwolf et al. (2022) shows that several representative OOD detection methods that optimize an objective that includes predictions on auxiliary OOD data are equivalent to the binary discriminator. Compared to Zhang et al. (2021); Morteza and Li (2022); Fang et al. (2022), our paper mainly focuses on the case that the auxiliary OOD data are available. Using the auxiliary OOD data, we can weaken the strong conditions proposed by Fang et al. (2022) and provide more reasonable and practical learning bounds for OOD detection. Compared to Bitterwolf et al. (2022), our theory mainly focuses on the learnability of OOD detection in the outlier exposure case and provides theoretical support to our practical method.

B Notations

In this section, we summarize the important notations in Table 3.

Table 3: Main notations and their descriptions.

Notation	Description
Spaces	
$\mathcal{X}$ and $\mathcal{Y}$	the feature space and the ID label space $\{1, \ldots, C\}$
$\mathcal{W}$	the parameter space
$\mathfrak{D}$	the distribution space
$\mathcal{E}$	the embedding space
Distributions	
$X_\mathrm{I}, X_\mathrm{A}, X_\mathrm{O}$	ID feature, auxiliary OOD feature, and real OOD feature
Y_I and Y_O	ID label and OOD label random variable
$D_{X_\mathrm{I} Y_\mathrm{I}}$ and $D_{X_\mathrm{O} Y_\mathrm{O}}$	ID joint distribution and OOD joint distribution
D_{X_A}	the auxiliary OOD distribution
δ	the dirac measure
Data and Models	
S and T	ID training data and auxiliary OOD training data
n and m	the number of ID data and the number of auxiliary OOD data
$\mathbf{x}_\mathrm{I}$ and $\mathbf{x}_\mathrm{A}$	ID data and auxiliary OOD data
y_I	ID label
$\mathbf{f_w}$	the model: $\mathcal{X} \to \mathbb{R}^C$, parameterized by $\mathbf{w} \in \mathcal{W}$
$\mathbf{e}$ and $\mathbf{h}$	the feature extractor and the classifier
$s(\cdot; \mathbf{f})$	the scoring function: $\mathcal{X} \to \mathbb{R}$
$g_\lambda(\cdot)$	the OOD detector: $\mathcal{X} \to \{\mathrm{ID}, \mathrm{OOD}\}$, with threshold λ
Distances	
$c(\cdot, \cdot)$	the cost function: $\mathcal{X} \times \mathcal{X} \to \mathbb{R}_+$
$d(\cdot, \cdot)$	the distance between two distributions: $\mathfrak{D} \times \mathfrak{D} \to \mathbb{R}_+$
W_c	the Wasserstein-1 distance: $\mathfrak{D} \times \mathfrak{D} \to \mathbb{R}_+$
ρ	the radius of the Wasserstein ball
$\|\cdot\|_p$	l_p norm
Loss and Risk	
ℓ and ℓ_OE	ID loss function and OOD loss function
$R_\mathrm{I}(\mathbf{w})$ and $\widehat{R}_\mathrm{I}(\mathbf{w})$	the expected risk and the empirical risk corresponding to $D_{X_\mathrm{I} Y_\mathrm{I}}$
$R_\mathrm{A}(\mathbf{w})$ and $\widehat{R}_\mathrm{A}(\mathbf{w})$	the expected risk and the empirical risk corresponding to D_{X_A}
$R_\mathrm{O}(\mathbf{w})$	the expected risk corresponding to D_{X_O}
$R_D(\mathbf{w})$	the real detection risk corresponding to D
$\phi_\gamma(\mathbf{w}; \mathbf{x})$	the surrogate function
$R_\mathrm{O}(\mathbf{w}; \rho)$ and $\widehat{R}_\mathrm{O}(\mathbf{w}; \rho)$	the expected DAL risk and the empirical one corresponding to D_{X_A}
$R_D(\mathbf{w}; \rho)$ and $\widehat{R}_D(\mathbf{w}; \rho)$	the expected DAL risk and the empirical one corresponding to D
Hypothesis Space	
$\mathcal{F}$ and $\mathcal{F}_\mathrm{OE}$	the model classes with respect to ℓ and ℓ_OE
$\mathcal{N}(\cdot, \epsilon, L^\infty)$	the covering number

C Proofs of Theorems

We provide the detailed proofs for our theoretical results in Sections 4.1.

C.1 Covering Number

We use the covering number for the model classes in our derivation. Here, we give the formal definition.

Definition 2 (ϵ-covering (Vershynin, 2018))**.** Let $(V, \|\cdot\|)$ be a normed space, $\Theta \subset V$, and $B(\cdot, \epsilon)$ the ball of radius ϵ. Then $\{V_1, \ldots, V_N\}$ is an ϵ-covering of Θ if $\Theta \subset \bigcup_{i=1}^{N} B(V_i, \epsilon)$, or equivalently, $\forall \theta \in \Theta, \exists i$ such that $\|\theta - V_i\| \leq \epsilon$.

Upon our definition of ϵ-covering, the covering number is the minimal number of ϵ-balls one needs to cover Θ.

Definition 3 (Covering Number (Vershynin, 2018))**.**

$$\mathcal{N}(\Theta, \|\cdot\|, \epsilon) = \min\{n : \exists \ \epsilon\text{-covering over } \Theta \text{ of size } n\}.$$

C.2 Proof of Lemma 1

Proof of Lemma 1. Because of $D_{X_A} \in \mathfrak{D}$, according to the definite of infimum, it is clear that

$$\inf_{D_{X'} \in \mathfrak{D}} d(D_{X'}, D_{X_O}) \leq d(D_{X_A}, D_{X_O}).$$

To prove the second result, we consider a special distribution D', which is defined as follows: for some $u \in [0, 1]$,

$$D' = (1 - u)D_{X_O} + uD_{X_A}.$$

Because $c(\cdot, \cdot)$ is a continuous metric, Kantorovich–Rubinstein duality (Villani, 2021) implies that

$$\begin{aligned}
\mathrm{W}_c(D', D_{X_O}) &= \sup_{\|f\|_{\mathrm{Lip}} \leq 1} \int_{\mathcal{X}} f(\mathbf{x}) \mathrm{d}D'(\mathbf{x}) - \int_{\mathcal{X}} f(\mathbf{x}) \mathrm{d}D_{X_O}(\mathbf{x}) \\
&= u \sup_{\|f\|_{\mathrm{Lip}} \leq 1} \int_{\mathcal{X}} f(\mathbf{x}) \mathrm{d}D_{X_A}(\mathbf{x}) - \int_{\mathcal{X}} f(\mathbf{x}) \mathrm{d}D_{X_O}(\mathbf{x}) \\
&= u\mathrm{W}_c(D_{X_A}, D_{X_O})
\end{aligned}$$

Similarly, we can obtain that

$$\mathrm{W}_c(D', D_{X_A}) = (1 - u)\mathrm{W}_c(D_{X_A}, D_{X_O})$$

Case 1. If $\mathrm{W}_c(D_{X_A}, D_{X_O}) \leq \rho$, then it is clear that

$$\inf_{D_{X'} \in \mathfrak{D}} \mathrm{W}_c(D_{X'}, D_{X_O}) \leq \max\{\mathrm{W}_c(D_{X_A}, D_{X_O}) - \rho, 0\}.$$

Case 2. If $\mathrm{W}_c(D_{X_A}, D_{X_O}) > \rho$, then we set $u = 1 - \rho/\mathrm{W}_c(D_{X_A}, D_{X_O})$. Therefore,

$$\mathrm{W}_c(D', D_{X_A}) = \rho, \qquad \mathrm{W}_c(D', D_{X_O}) = \mathrm{W}_c(D_{X_A}, D_{X_O}) - \rho,$$

which implies that

$$\inf_{D_{X'} \in \mathfrak{D}} \mathrm{W}_c(D_{X'}, D_{X_O}) \leq \mathrm{W}_c(D', D_{X_O}) = \mathrm{W}_c(D_{X_A}, D_{X_O}) - \rho \leq \max\{\mathrm{W}_c(D_{X_A}, D_{X_O}) - \rho, 0\}.$$

We have completed this proof by combining Cases 1 and 2. □

C.3 Proof of Theorem 1

Proof of Theorem 1. One can find a similar proof from Blanchet et al. (2019); Blanchet and KarthyekRajhaaA. (2016); Sinha et al. (2018). We omit it here. □

C.4 Proof of Theorem 2

Proof of Theorem 2. We first recall the notations as follows:

$$R_{\mathrm{I}}(\mathbf{w}) = \mathbb{E}_{(\mathbf{x},y)\sim D_{X_{\mathrm{I}}Y_{\mathrm{I}}}} \ell(\mathbf{f}_{\mathbf{w}}; \mathbf{x}, y),$$

$$\widehat{R}_{\mathrm{I}}(\mathbf{w}) = \frac{1}{n} \sum_{i=1}^{n} \ell(\mathbf{f}_{\mathbf{w}}; \mathbf{x}_{\mathrm{I}}^{i}, y_{\mathrm{I}}^{i}),$$

$$R_{\mathrm{O}}(\mathbf{w}; \rho) = \sup_{\mathrm{W}_c(D_{X'}, D_{X_{\mathrm{A}}}) \leq \rho} \mathbb{E}_{\mathbf{x}\sim D_{X'}} \ell_{\mathrm{OE}}(\mathbf{f}_{\mathbf{w}}; \mathbf{x}),$$

$$\widehat{R}_{\mathrm{O}}(\mathbf{w}; \rho) = \sup_{\mathrm{W}_c(D_{X'}, \widehat{D}_{X_{\mathrm{A}}}) \leq \rho} \mathbb{E}_{\mathbf{x}\sim D_{X'}} \ell_{\mathrm{OE}}(\mathbf{f}_{\mathbf{w}}; \mathbf{x}).$$

Let $\mathbf{w}^*$ be the solution of $\min_{\mathbf{w}\in\mathcal{W}} R_D(\mathbf{w}; \rho)$. Then

$$R_D(\widehat{\mathbf{w}}; \rho) - R_D(\mathbf{w}^*; \rho)$$
$$\leq R_D(\widehat{\mathbf{w}}; \rho) - \widehat{R}_D(\widehat{\mathbf{w}}; \rho) + \widehat{R}_D(\widehat{\mathbf{w}}; \rho) - R_D(\mathbf{w}^*; \rho) + \widehat{R}_D(\mathbf{w}^*; \rho) - \widehat{R}_D(\mathbf{w}^*; \rho)$$
$$\leq [R_{\mathrm{I}}(\widehat{\mathbf{w}}) - R_{\mathrm{I}}(\mathbf{w}^*)] + \alpha[R_{\mathrm{O}}(\widehat{\mathbf{w}}; \rho) - R_{\mathrm{O}}(\mathbf{w}^*; \rho)] - [\widehat{R}_{\mathrm{I}}(\widehat{\mathbf{w}}) - \widehat{R}_{\mathrm{I}}(\mathbf{w}^*)] - \alpha[\widehat{R}_{\mathrm{O}}(\widehat{\mathbf{w}}; \rho) - \widehat{R}_{\mathrm{O}}(\mathbf{w}^*; \rho)]$$
$$= [R_{\mathrm{I}}(\widehat{\mathbf{w}}) - \widehat{R}_{\mathrm{I}}(\widehat{\mathbf{w}})] + \alpha[R_{\mathrm{O}}(\widehat{\mathbf{w}}; \rho) - \widehat{R}_{\mathrm{O}}(\widehat{\mathbf{w}}; \rho)] - [R_{\mathrm{I}}(\mathbf{w}^*) - \widehat{R}_{\mathrm{I}}(\mathbf{w}^*)] - \alpha[R_{\mathrm{O}}(\mathbf{w}^*; \rho) - \widehat{R}_{\mathrm{O}}(\mathbf{w}^*; \rho)].$$
$$(12)$$

By Lemmas 4 and 9, we have that with the probability at least $1 - 2e^{-t} > 0$, for any $\rho > 0$,

$$[R_{\mathrm{I}}(\widehat{\mathbf{w}}) - \widehat{R}_{\mathrm{I}}(\widehat{\mathbf{w}})] + \alpha[R_{\mathrm{O}}(\widehat{\mathbf{w}}; \rho) - \widehat{R}_{\mathrm{O}}(\widehat{\mathbf{w}}; \rho)]$$
$$\leq \frac{b_0 M_\ell}{\sqrt{n}} \int_0^1 \sqrt{\log \mathcal{N}(\mathcal{F}, M_\ell \epsilon, L^\infty)} d\epsilon \qquad (13)$$
$$+ \alpha b_1 \sqrt{\frac{M_{\ell_{\mathrm{OE}}}^3}{\rho^2 m}} \int_0^1 \sqrt{\log \mathcal{N}(\mathcal{F}_{\mathrm{OE}}, M_{\ell_{\mathrm{OE}}} \epsilon, L^\infty)} d\epsilon + \alpha b_2 M_{\ell_{\mathrm{OE}}} \sqrt{\frac{2t}{m}} + M_\ell \sqrt{\frac{2t}{n}}.$$

By Lemmas 8 and 10, we have that with the probability at least $1 - 2e^{-t} > 0$, for any $\rho > 0$,

$$[R_{\mathrm{I}}(\mathbf{w}^*) - \widehat{R}_{\mathrm{I}}(\mathbf{w}^*)] + \alpha[R_{\mathrm{O}}(\mathbf{w}^*; \rho) - \widehat{R}_{\mathrm{O}}(\mathbf{w}^*; \rho)] \leq M_\ell \sqrt{\frac{2t}{n}} + 2\alpha M_{\ell_{\mathrm{OE}}} \sqrt{\frac{2t}{m}}. \qquad (14)$$

Combining Eqs. (12), (13) and (14), we have that with the probability at least $1 - 4e^{-t} > 0$, for any $\rho > 0$,

$$R_D(\widehat{\mathbf{w}}; \rho) - R_D(\mathbf{w}^*; \rho)$$
$$\leq \frac{b_0 M_\ell}{\sqrt{n}} \int_0^1 \sqrt{\log \mathcal{N}(\mathcal{F}, M_\ell \epsilon, L^\infty)} d\epsilon$$
$$+ \alpha b_1 \sqrt{\frac{M_{\ell_{\mathrm{OE}}}^3}{\rho^2 m}} \int_0^1 \sqrt{\log \mathcal{N}(\mathcal{F}_{\mathrm{OE}}, M_{\ell_{\mathrm{OE}}} \epsilon, L^\infty)} d\epsilon + 2M_\ell \sqrt{\frac{2t}{n}} + b_2 \alpha M_{\ell_{\mathrm{OE}}} \sqrt{\frac{2t}{m}},$$

where b_0, b_1 and b_2 are uniform constants. ∎

Remark 4. One can prove that the cross-entropy and the exponential losses are bounded and lipschitz w.r.t. $\mathbf{w}$ for deep models with softmax outputs (Golowich et al., 2018), if

- activation functions are 1-Lipschitz;

- inputs are from bounded feature space $\mathcal{X}$;

- the parameter space $\mathcal{W}$ is bounded (e.g., with regularization).

More specifically, when the F-norm bounds parameters, the softmax output is continuous and never attains infinity. If we further assume that inputs are from a bounded feature space, then the model is a continuous function over the bounded space, implying that model outputs have upper and lower bounds. Thus, the cross-entropy and the exponential loss can be bounded in practice, and our assumptions are practical.

C.5 Corollary 1

Corollary 1. *Given the same conditions in Theorem 2, if*

- *$\ell_{\mathrm{OE}}(\mathbf{f_w};\mathbf{x})$ is L_{OE}-Lipschitz w.r.t. norm $\|\cdot\|$, i.e.,*

$$|\ell_{\mathrm{OE}}(\mathbf{f_w};\mathbf{x}) - \ell_{\mathrm{OE}}(\mathbf{f_{w'}};\mathbf{x})| \leq L_{\mathrm{OE}}\|\mathbf{w}-\mathbf{w'}\|,$$

- *$\ell_{\mathrm{OE}}(\mathbf{f_w};\mathbf{x})$ is L_c-Lipschitz w.r.t. $c(\cdot,\cdot)$, i.e.,*

$$|\ell_{\mathrm{OE}}(\mathbf{f_w};\mathbf{x}) - \ell_{\mathrm{OE}}(\mathbf{f_w};\mathbf{x'})| \leq L_c c(\mathbf{x},\mathbf{x'}),$$

- *$\ell(\mathbf{f_w};\mathbf{x},y)$ is L-Lipschitz w.r.t. norm $\|\cdot\|$, i.e.,*

$$|\ell(\mathbf{f_w};\mathbf{x},y) - \ell(\mathbf{f_{w'}};\mathbf{x},y)| \leq L\|\mathbf{w}-\mathbf{w'}\|,$$

- *the parameter space $\mathcal{W}\subset\mathbb{R}^{d'}$ satisfies that*

$$\mathrm{diam}(\mathcal{W}) = \sup_{\mathbf{w},\mathbf{w'}\in\mathcal{W}}\|\mathbf{w}-\mathbf{w'}\| < +\infty.$$

Let $\widehat{\mathbf{w}}$ be the optimal solution of Eq. (8), i.e.,

$$\widehat{\mathbf{w}} \in \arg\min_{\mathbf{w}\in\mathcal{W}} \widehat{R}_D(\mathbf{w};\rho).$$

With the probability at least $1 - 4e^{-t} > 0$, for any $\rho > 0$,

$$R_D(\widehat{\mathbf{w}};\rho) - \min_{\mathbf{w}\in\mathcal{W}} R_D(\mathbf{w};\rho) \leq \tilde{\epsilon}(n,m;t),$$

where

$$\begin{aligned}
\tilde{\epsilon}(n,m;t) =& b_0\sqrt{\frac{M_\ell \mathrm{diam}(\mathcal{W})Ld'}{n}} \\
&+ \alpha b_1 \min\{L_c, \frac{M_{\ell_{\mathrm{OE}}}}{\rho}\}\sqrt{\frac{\mathrm{diam}(\mathcal{W})L_{\mathrm{OE}}d'}{m}} \\
&+ 2M_\ell\sqrt{\frac{2t}{n}} + \alpha b_2 M_{\ell_{\mathrm{OE}}}\sqrt{\frac{2t}{m}},
\end{aligned}$$

here b_0, b_1 and b_2 are uniform constants.

Proof of Corollary 1. By Lemmas 7 and 11, we have that with the probability at least $1 - 2e^{-t} > 0$, for any $\rho > 0$,

$$\begin{aligned}
&[R_{\mathrm{I}}(\widehat{\mathbf{w}}) - \widehat{R}_{\mathrm{I}}(\widehat{\mathbf{w}})] + \alpha[R_{\mathrm{O}}(\widehat{\mathbf{w}};\rho) - \widehat{R}_{\mathrm{O}}(\widehat{\mathbf{w}};\rho)] \\
\leq& \Big[b_0\sqrt{\frac{M_\ell \mathrm{diam}(\mathcal{W})Ld'}{n}} + M_\ell\sqrt{\frac{2t}{n}}\Big] + \alpha b_1 \min\{L_c, \frac{M_{\ell_{\mathrm{OE}}}}{\rho}\}\sqrt{\frac{\mathrm{diam}(\mathcal{W})L_{\mathrm{OE}}d'}{m}} + \alpha b_2 M_{\ell_{\mathrm{OE}}}\sqrt{\frac{t}{m}}
\end{aligned}$$
(15)

By Lemmas 8 and 10, we have that with the probability at least $1 - 2e^{-t} > 0$, for any $\rho > 0$,

$$[R_{\mathrm{I}}(\mathbf{w}^*) - \widehat{R}_{\mathrm{I}}(\mathbf{w}^*)] + \alpha[R_{\mathrm{O}}(\mathbf{w}^*;\rho) - \widehat{R}_{\mathrm{O}}(\mathbf{w}^*;\rho)] \leq M_\ell\sqrt{\frac{2t}{n}} + 2\alpha M_{\ell_{\mathrm{OE}}}\sqrt{\frac{2t}{m}}. \quad (16)$$

Using Eqs. (15), (16) and Eq. (12), we know that with the probability at least $1 - 4e^{-t} > 0$, for any $\rho > 0$,

$$\begin{aligned}
&R_D(\widehat{\mathbf{w}};\rho) - \min_{\mathbf{w}\in\mathcal{W}} R_D(\mathbf{w};\rho) \\
\leq& b_0\sqrt{\frac{M_\ell \mathrm{diam}(\mathcal{W})Ld'}{n}} + \alpha b_1 \min\{L_c, \frac{M_{\ell_{\mathrm{OE}}}}{\rho}\}\sqrt{\frac{\mathrm{diam}(\mathcal{W})L_{\mathrm{OE}}d'}{m}} + 2M_\ell\sqrt{\frac{2t}{n}} + \alpha b_2 M_{\ell_{\mathrm{OE}}}\sqrt{\frac{2t}{m}},
\end{aligned}$$

where b_0, b_1 and b_2 are uniform constants. $\qquad\square$

C.6 Proof of Theorem 3

Proof of Theorem 3. Consider
$$R_D(\widehat{\mathbf{w}}) - R_D(\widehat{\mathbf{w}}; \rho).$$

It is clear that
$$R_D(\widehat{\mathbf{w}}) - R_D(\widehat{\mathbf{w}}; \rho) = \alpha[R_O(\widehat{\mathbf{w}}) - R_O(\widehat{\mathbf{w}}; \rho)].$$

Let $D' = (1-u)D_{X_O} + uD_{X_A}$ and
$$\rho_O = W_c(D_{X_O}, D_{X_A}).$$

Because $c(\cdot, \cdot)$ is a continuous metric, Kantorovich–Rubinstein duality Villani (2021) implies that

$$
\begin{aligned}
& W_c(D', D_{X_A}) \\
&= \sup_{\|f\|_{\mathrm{Lip}} \le 1} \int_{\mathcal{X}} f(\mathbf{x}) \mathrm{d}D'(\mathbf{x}) - \int_{\mathcal{X}} f(\mathbf{x}) \mathrm{d}D_{X_A}(\mathbf{x}) \\
&= (1-u) \sup_{\|f\|_{\mathrm{Lip}} \le 1} \int_{\mathcal{X}} f(\mathbf{x}) \mathrm{d}D_{X_O}(\mathbf{x}) - \int_{\mathcal{X}} f(\mathbf{x}) \mathrm{d}D_{X_A}(\mathbf{x}) \\
&= (1-u) W_c(D_{X_O}, D_{X_A}) \\
&= (1-u)\rho_O
\end{aligned}
$$

Let
$$u = 1 - \frac{\rho}{\rho_O}.$$

Case 1. If $\rho \ge \rho_O$, then
$$R_D(\widehat{\mathbf{w}}) \le R_D(\widehat{\mathbf{w}}; \rho)$$

Case 2. If $\rho < \rho_O$, then by Lemma 6
$$R_O(\widehat{\mathbf{w}}) - R_O(\widehat{\mathbf{w}}; \rho) \le R_O(\widehat{\mathbf{w}}) - \mathbb{E}_{\mathbf{x} \sim D'} \ell_{\mathrm{OE}}(\mathbf{f}_{\mathbf{w}}; \mathbf{x}) \le L_c(\rho_O - \rho),$$

By Cases 1 and 2, we have shown that
$$R_D(\widehat{\mathbf{w}}) - R_D(\widehat{\mathbf{w}}; \rho) \le \alpha L_c \max\{W_c(D_{X_o}, D_{X_A}) - \rho, 0\}.$$

Then by Theorem 2, we complete this proof. $\qquad\square$

D   Necessary Lemmas

Lemma 2. *Assume that*

- $|\ell_{\mathrm{OE}}(\mathbf{f_w}; \mathbf{x})| \leq M_{\ell_{\mathrm{OE}}}$,

- $c : \mathcal{X} \times \mathcal{X} \to \mathbb{R}_+$ *is a continuous metric,*

then

- $|\phi_\gamma(\mathbf{w}; \mathbf{x})| \leq M_{\ell_{\mathrm{OE}}}$,

- *for some* $\mathbf{w}_0 \in \mathcal{W}$ *and* $\epsilon > 0$, *when* γ_ϵ ($\gamma_\epsilon \geq 0$) *satisfies the following condition:*

$$\gamma_\epsilon \rho + \mathbb{E}_{\mathbf{x} \sim D} \phi_{\gamma_\epsilon}(\mathbf{w}_0; \mathbf{x}) \leq \inf_{\gamma \geq 0} [\gamma \rho + \mathbb{E}_{\mathbf{x} \sim D} \phi_\gamma(\mathbf{w}_0; \mathbf{x})] + \epsilon,$$

then

$$\gamma_\epsilon \leq \frac{2M_{\ell_{\mathrm{OE}}} + \epsilon}{\rho}.$$

Proof of Lemma 2. **First**, we prove: $|\phi_\gamma(\mathbf{w}; \mathbf{x})| \leq M_{\ell_{\mathrm{OE}}}$.

Because $\phi_\gamma(\mathbf{w}; \mathbf{x}) = \sup_{\mathbf{x}' \in \mathcal{X}} \{\ell_{\mathrm{OE}}(\mathbf{f_w}; \mathbf{x}') - \gamma c(\mathbf{x}', \mathbf{x})\}$ and $c(\mathbf{x}, \mathbf{x}') \geq 0$, it is clear that

$$\phi_\gamma(\mathbf{w}; \mathbf{x}) \leq \sup_{\mathbf{x}' \in \mathcal{X}} \ell_{\mathrm{OE}}(\mathbf{f_w}; \mathbf{x}') \leq M_{\ell_{\mathrm{OE}}}.$$

In addition, because $c(\mathbf{x}, \mathbf{x}) = 0$, then

$$\phi_\gamma(\mathbf{w}; \mathbf{x}) \geq \ell_{\mathrm{OE}}(\mathbf{w}; \mathbf{x}) \geq -M_{\ell_{\mathrm{OE}}}.$$

Above inequalities have indicated that

$$|\phi_\gamma(\mathbf{w}; \mathbf{x})| \leq M_{\ell_{\mathrm{OE}}}.$$

Second, we prove that

$$\gamma_\epsilon \leq \frac{2M_{\ell_{\mathrm{OE}}} + \epsilon}{\rho}.$$

By the dual theorem in Blanchet et al. (2019); Blanchet and KarthyekRajhaaA. (2016); Sinha et al. (2018), we can obtain that

$$\inf_{\gamma \geq 0} [\gamma \rho + \mathbb{E}_{\mathbf{x} \sim D} \phi_\gamma(\mathbf{w}_0; \mathbf{x})] = \sup_{\mathrm{W}_c(D', D) \leq \rho} \mathbb{E}_{\mathbf{x} \sim D'} \ell_{\mathrm{OE}}(\mathbf{f}_{\mathbf{w}_0}; \mathbf{x}) \leq M_{\ell_{\mathrm{OE}}},$$

which implies that

$$\gamma_\epsilon \rho \leq M_{\ell_{\mathrm{OE}}} + \epsilon - \mathbb{E}_{\mathbf{x} \sim D} \phi_\gamma(\mathbf{w}_0; \mathbf{x}) \leq 2M_{\ell_{\mathrm{OE}}} + \epsilon.$$

Therefore,

$$\gamma_\epsilon \leq \frac{2M_{\ell_{\mathrm{OE}}} + \epsilon}{\rho}.$$

$\square$

Lemma 3 (Theorem 3 in Sinha et al. (2018)). *Given the same assumptions in Theorem 2, then with the probability at least* $1 - e^{-t} > 0$, *for any* $\gamma \geq 0$, $\rho \geq 0$ *and* $\mathbf{w} \in \mathcal{W}$,

$$\sup_{\mathrm{W}_c(D_{X'}, D_{X_A}) \leq \rho} \mathbb{E}_{\mathbf{x} \sim D_{X'}} \ell_{\mathrm{OE}}(\mathbf{f_w}; \mathbf{x})$$

$$\leq \gamma \rho + \frac{1}{m} \sum_{i=1}^{m} \phi_\gamma(\mathbf{w}; \mathbf{x}_A^i) + b_2 M_{\ell_{\mathrm{OE}}} \sqrt{\frac{t}{m}} + \gamma b_1 \sqrt{\frac{M_{\ell_{\mathrm{OE}}}}{m}} \int_0^1 \sqrt{\log \mathcal{N}(\mathcal{F}_{\mathrm{OE}}, M_{\ell_{\mathrm{OE}}} \epsilon, L^\infty)} d\epsilon,$$

where b_1 *and* b_2 *are uniform constants.*

Proof of Lemma 3. This lemma is following Theorem 3 in Sinha et al. (2018). $\square$

Lemma 4. *Given the same assumptions in Theorem 2, then with the probability at least $1 - e^{-t} > 0$, for any $\rho > 0$ and $\mathbf{w} \in \mathcal{W}$, we have*

$$\sup_{\mathrm{W}_c(D_{X'}, D_{X_\mathrm{A}}) \leq \rho} \mathbb{E}_{\mathbf{x} \sim D_\mathrm{O}} \ell_\mathrm{OE}(\mathbf{f_w}; \mathbf{x})$$

$$\leq \sup_{\mathrm{W}_c(D_{X'}, \widehat{D}_{X_\mathrm{A}}) \leq \rho} \mathbb{E}_{\mathbf{x} \sim D_\mathrm{O}} \ell_\mathrm{OE}(\mathbf{f_w}; \mathbf{x}) + b_2 M_{\ell_\mathrm{OE}} \sqrt{\frac{t}{m}} + b_1 \sqrt{\frac{M_{\ell_\mathrm{OE}}^3}{\rho^2 m}} \int_0^1 \sqrt{\log \mathcal{N}(\mathcal{F}_\mathrm{OE}, M_{\ell_\mathrm{OE}} \epsilon, L^\infty)} \mathrm{d}\epsilon,$$

where b_1 and b_2 are uniform constants.

Proof of Lemma 4. By Lemma 3, we know that with the probability at least $1 - e^{-t} > 0$, for any $\frac{3M_{\ell_\mathrm{OE}}}{\rho} \geq \gamma \geq 0$, $\rho \geq 0$ and $\mathbf{w} \in \mathcal{W}$, we have

$$\sup_{\mathrm{W}_c(D_{X'}, D_{X_\mathrm{A}}) \leq \rho} \mathbb{E}_{\mathbf{x} \sim D_{X'}} \ell_\mathrm{OE}(\mathbf{f_w}; \mathbf{x})$$

$$\leq \gamma \rho + \frac{1}{m} \sum_{i=1}^m \phi_\gamma(\mathbf{w}; \mathbf{x}_\mathrm{A}^i) + b_2 M_{\ell_\mathrm{OE}} \sqrt{\frac{t}{m}} + b_1 \sqrt{\frac{M_{\ell_\mathrm{OE}}^3}{\rho^2 m}} \int_0^1 \sqrt{\log \mathcal{N}(\mathcal{F}_\mathrm{OE}, M_{\ell_\mathrm{OE}} \epsilon, L^\infty)} \mathrm{d}\epsilon,$$

where b_1 and b_2 are uniform constants.

The above bound and Lemma 2 imply that with the probability at least $1 - e^{-t} > 0$, for any $\rho \geq 0$ and $\mathbf{w} \in \mathcal{W}$, we have

$$\sup_{\mathrm{W}_c(D_{X'}, D_{X_\mathrm{A}}) \leq \rho} \mathbb{E}_{\mathbf{x} \sim D_{X'}} \ell_\mathrm{OE}(\mathbf{f_w}; \mathbf{x})$$

$$\leq \inf_{\gamma \geq 0} \left(\gamma \rho + \frac{1}{m} \sum_{i=1}^m \phi_\gamma(\mathbf{w}; \mathbf{x}_\mathrm{A}^i) \right) + b_2 M_{\ell_\mathrm{OE}} \sqrt{\frac{t}{m}} + b_1 \sqrt{\frac{M_{\ell_\mathrm{OE}}^3}{\rho^2 m}} \int_0^1 \sqrt{\log \mathcal{N}(\mathcal{F}_\mathrm{OE}, M_{\ell_\mathrm{OE}} \epsilon, L^\infty)} \mathrm{d}\epsilon.$$

Combining the above inequality with the following equation:

$$\inf_{\gamma \geq 0} \left(\gamma \rho + \frac{1}{m} \sum_{i=1}^m \phi_\gamma(\mathbf{w}; \mathbf{x}_\mathrm{A}^i) \right) = \sup_{\mathrm{W}_c(D_{X'}, \widehat{D}_{X_\mathrm{A}}) \leq \rho} \mathbb{E}_{\mathbf{x} \sim D_{X'}} \ell_\mathrm{OE}(\mathbf{f_w}; \mathbf{x}),$$

we complete this proof. $\qquad\square$

Lemma 5. *Given the same assumptions in Lemma 4, if $\ell_\mathrm{OE}(\mathbf{f_w}; \mathbf{x})$ is a L_OE-Lipschitz function w.r.t. norm $\| \cdot \|$ for all $\mathbf{x} \in \mathcal{X}$ and the parameter space $\mathcal{W} \subset \mathbb{R}^{d'}$ satisfies that $\mathrm{diam}(\mathcal{W}) = \sup_{\mathbf{w}, \mathbf{w}' \in \mathcal{W}} \| \mathbf{w} - \mathbf{w}' \| < +\infty$, then with the probability at least $1 - e^{-t} > 0$, for any $\rho > 0$ and $\mathbf{w} \in \mathcal{W}$,*

$$\sup_{\mathrm{W}_c(D_{X'}, D_{X_\mathrm{A}}) \leq \rho} \mathbb{E}_{\mathbf{x} \sim D_\mathrm{O}} \ell_\mathrm{OE}(\mathbf{f_w}; \mathbf{x})$$

$$\leq \sup_{\mathrm{W}_c(D_{X'}, \widehat{D}_{X_\mathrm{A}}) \leq \rho} \mathbb{E}_{\mathbf{x} \sim D_\mathrm{O}} \ell_\mathrm{OE}(\mathbf{f_w}; \mathbf{x}) + b_2 M_{\ell_\mathrm{OE}} \sqrt{\frac{t}{m}} + b_1 M_{\ell_\mathrm{OE}} \sqrt{\frac{\mathrm{diam}(\mathcal{W}) L_\mathrm{OE} d'}{\rho^2 m}},$$

where b_1 and b_2 are uniform constants.

Proof. The proof is similar to Corollary 1 in Sinha et al. (2018). Note that

$$\mathcal{F}_\mathrm{OE} = \{\ell_\mathrm{OE}(\mathbf{f_w}; \mathbf{x}) : \mathbf{w} \in \mathcal{W}\},$$

and $\ell_\mathrm{OE}(\mathbf{f_w}; \mathbf{x})$ is L_OE-Lipschitz w.r.t. norm $\| \cdot \|$, therefore,

$$\mathcal{N}(\mathcal{F}_\mathrm{OE}, M_{\ell_\mathrm{OE}} \epsilon, L^\infty) \leq \mathcal{N}(\mathcal{W}, M_{\ell_\mathrm{OE}} \epsilon / L_\mathrm{OE}, \| \cdot \|) \leq (1 + \frac{\mathrm{diam}(\mathcal{W}) L_\mathrm{OE}}{M_{\ell_\mathrm{OE}} \epsilon})^{d'},$$

which implies that

$$\int_0^1 \sqrt{\log(\mathcal{N}(\mathcal{F}_{\mathrm{OE}}, M_{\ell_{\mathrm{OE}}}\epsilon, L^\infty))}\mathrm{d}\epsilon$$

$$\leq \sqrt{d'}\int_0^1 \sqrt{\log(1+\frac{\mathrm{diam}(\mathcal{W})L_{\mathrm{OE}}}{M_{\ell_{\mathrm{OE}}}\epsilon})}\mathrm{d}\epsilon$$

$$\leq \sqrt{d'}\int_0^1 \sqrt{\frac{\mathrm{diam}(\mathcal{W})L_{\mathrm{OE}}}{M_{\ell_{\mathrm{OE}}}\epsilon}}\mathrm{d}\epsilon = 2\sqrt{\frac{\mathrm{diam}(\mathcal{W})L_{\mathrm{OE}}d'}{M_{\ell_{\mathrm{OE}}}}}.$$

By Lemma 4, we obtain that there exist two uniform constants such that with the probability at least $1 - e^{-t} > 0$,

$$\sup_{\mathrm{W}_c(D_{X'}, D_{X_{\mathrm{A}}})\leq\rho} \mathbb{E}_{\mathbf{x}\sim D_{\mathrm{O}}}\ell_{\mathrm{OE}}(\mathbf{f_w};\mathbf{x})$$

$$\leq \sup_{\mathrm{W}_c(D_{X'}, \widehat{D}_{X_{\mathrm{A}}})\leq\rho} \mathbb{E}_{\mathbf{x}\sim D_{\mathrm{O}}}\ell_{\mathrm{OE}}(\mathbf{f_w};\mathbf{x}) + b_2 M_{\ell_{\mathrm{OE}}}\sqrt{\frac{t}{m}} + b_1 M_{\ell_{\mathrm{OE}}}\sqrt{\frac{\mathrm{diam}(\mathcal{W})L_{\mathrm{OE}}d'}{\rho^2 m}},$$

where b_1 and b_2 are uniform constants. $\qquad\square$

Lemma 6. *Given the same assumptions in Theorem 2, and for any $\mathbf{w} \in \mathcal{W}$ and any $\mathbf{x}, \mathbf{x}' \in \mathcal{X}$,*

$$|\ell_{\mathrm{OE}}(\mathbf{f_w};\mathbf{x}) - \ell_{\mathrm{OE}}(\mathbf{f_w};\mathbf{x}')| \leq L_c c(\mathbf{x}, \mathbf{x}'),$$

then for any $\delta \geq 0$,

$$\sup_{\mathrm{W}_c(D_{X'}, D_{X_{\mathrm{A}}})\leq\rho+\delta} \mathbb{E}_{\mathbf{x}\sim D_{X'}}\ell_{\mathrm{OE}}(\mathbf{f_w};\mathbf{x}) - \sup_{\mathrm{W}_c(D_{X'}, D_{X_{\mathrm{A}}})\leq\rho} \mathbb{E}_{\mathbf{x}\sim D_{X'}}\ell_{\mathrm{OE}}(\mathbf{f_w};\mathbf{x}) \leq L_c\delta.$$

Proof of Lemma 6. For each $\epsilon > 0$, we set $D_{X'}^{\delta,\epsilon}$ satisfies that

$$\sup_{\mathrm{W}_c(D_{X'}, D_{X_{\mathrm{A}}})\leq\rho+\delta} \mathbb{E}_{\mathbf{x}\sim D_{X'}}\ell_{\mathrm{OE}}(\mathbf{f_w};\mathbf{x}) \leq \mathbb{E}_{\mathbf{x}\sim D_{X'}^{\delta,\epsilon}}\ell_{\mathrm{OE}}(\mathbf{f_w};\mathbf{x}) + \epsilon,$$

and

$$\mathrm{W}_c(D_{X'}^{\delta,\epsilon}, D_{X_{\mathrm{A}}}) \leq \rho + \delta.$$

Case 1. If

$$\mathrm{W}_c(D_{X'}^{\delta,\epsilon}, D_{X_{\mathrm{A}}}) \leq \rho,$$

then

$$\sup_{\mathrm{W}_c(D_{X'}, D_{X_{\mathrm{A}}})\leq\rho+\delta} \mathbb{E}_{\mathbf{x}\sim D_{X'}}\ell_{\mathrm{OE}}(\mathbf{f_w};\mathbf{x}) - \sup_{\mathrm{W}_c(D_{X'}, D_{X_{\mathrm{A}}})\leq\rho} \mathbb{E}_{\mathbf{x}\sim D_{X'}}\ell_{\mathrm{OE}}(\mathbf{f_w};\mathbf{x}) \leq \epsilon.$$

Case 2. If

$$\mathrm{W}_c(D_{X'}^{\delta,\epsilon}, D_{X_{\mathrm{A}}}) > \rho,$$

then we consider a special distribution $D'_{X'}$, which is defined as follows: for some $u \in [0, 1]$,

$$D'_{X'} = (1-u)D_{X'}^{\delta,\epsilon} + u D_{X_{\mathrm{A}}}.$$

It is clear that

$$\mathrm{W}_c(D'_{X'}, D_{X_{\mathrm{A}}}) \leq (1-u)\mathrm{W}_c(D_{X'}^{\delta,\epsilon}, D_{X_{\mathrm{A}}}) \leq (1-u)(\rho+\delta).$$

hence, if we set $u = \delta/(\rho+\delta)$,

$$\mathrm{W}_c(D'_{X'}, D_{X_{\mathrm{A}}}) \leq \rho.$$

Because $c(\cdot, \cdot)$ is a metric, Kantorovich–Rubinstein duality Villani (2021) implies that

$$\mathrm{W}_c(D'_{X'}, D_{X'}^{\delta,\epsilon})$$

$$= \sup_{\|f\|_{\mathrm{Lip}}\leq 1} \int_{\mathcal{X}} f(\mathbf{x})\mathrm{d}D'_{X'}(\mathbf{x}) - \int_{\mathcal{X}} f(\mathbf{x})\mathrm{d}D_{X'}^{\delta,\epsilon}(\mathbf{x})$$

$$= u \sup_{\|f\|_{\mathrm{Lip}}\leq 1} \int_{\mathcal{X}} f(\mathbf{x})\mathrm{d}D_{X_{\mathrm{A}}}(\mathbf{x}) - \int_{\mathcal{X}} f(\mathbf{x})\mathrm{d}D_{X'}^{\delta,\epsilon}(\mathbf{x})$$

$$= u\mathrm{W}_c(D_{X_{\mathrm{A}}}, D_{X'}^{\delta,\epsilon})$$

$$= \delta$$

By Kantorovich–Rubinstein duality (Villani, 2021), we also obtain that

$$\sup_{\mathrm{W}_c(D_{X'},D_{X_{\mathrm{A}}})\leq\rho+\delta}\mathbb{E}_{\mathbf{x}\sim D_{X'}}\ell_{\mathrm{OE}}(\mathbf{f_w};\mathbf{x}) - \sup_{\mathrm{W}_c(D_{X'},D_{X_{\mathrm{A}}})\leq\rho}\mathbb{E}_{\mathbf{x}\sim D_{X'}}\ell_{\mathrm{OE}}(\mathbf{f_w};\mathbf{x})$$

$$\leq\mathbb{E}_{\mathbf{x}\sim D_{X'}^{\delta,\epsilon}}\ell_{\mathrm{OE}}(\mathbf{f_w};\mathbf{x}) - \mathbb{E}_{\mathbf{x}\sim D_{X'}'}\ell_{\mathrm{OE}}(\mathbf{f_w};\mathbf{x}) + \epsilon \leq L_c\delta + \epsilon,$$

which implies that

$$\sup_{\mathrm{W}_c(D_{X'},D_{X_{\mathrm{A}}})\leq\rho+\delta}\mathbb{E}_{\mathbf{x}\sim D_{X'}}\ell_{\mathrm{OE}}(\mathbf{f_w};\mathbf{x}) - \sup_{\mathrm{W}_c(D_{X'},D_{X_{\mathrm{A}}})\leq\rho}\mathbb{E}_{\mathbf{x}\sim D_{X'}}\ell_{\mathrm{OE}}(\mathbf{f_w};\mathbf{x}) \leq L_c\delta.$$

By Cases 1 and 2, we prove this lemma. $\qquad\square$

Lemma 7. *Given the same assumptions in Theorem 2, if*

- *$\ell_{\mathrm{OE}}(\cdot;\mathbf{x})$ is L_{OE}-Lipschitz w.r.t. norm $\|\cdot\|$ for all $\mathbf{x}\in\mathcal{X}$;*

- *the parameter space $\mathcal{W}\subset\mathbb{R}^{d'}$ satisfies that*

$$\mathrm{diam}(\mathcal{W}) = \sup_{\mathbf{w},\mathbf{w}'\in\mathcal{W}}\|\mathbf{w}-\mathbf{w}'\| < +\infty;$$

- *for each $\mathbf{w}\in\mathcal{W}$ and any $\mathbf{x},\mathbf{x}'\in\mathcal{X}$,*

$$|\ell_{\mathrm{OE}}(\mathbf{f_w};\mathbf{x}) - \ell_{\mathrm{OE}}(\mathbf{f_w};\mathbf{x}')| \leq L_c c(\mathbf{x},\mathbf{x}'),$$

then with the probability at least $1 - e^{-t} > 0$, for any $\rho > 0$ and $\mathbf{w}\in\mathcal{W}$,

$$\sup_{\mathrm{W}_c(D_{X'},D_{X_{\mathrm{A}}})\leq\rho}\mathbb{E}_{\mathbf{x}\sim D_{X'}}\ell_{\mathrm{OE}}(\mathbf{f_w};\mathbf{x})$$

$$\leq \sup_{\mathrm{W}_c(D_{X'},\widehat{D}_{X_{\mathrm{A}}})\leq\rho}\mathbb{E}_{\mathbf{x}\sim D_{X'}}\ell_{\mathrm{OE}}(\mathbf{f_w};\mathbf{x}) + b_2 M_{\ell_{\mathrm{OE}}}\sqrt{\frac{t}{m}} + b_1\min\{L_c,\frac{M_{\ell_{\mathrm{OE}}}}{\rho}\}\sqrt{\frac{\mathrm{diam}(\mathcal{W})L_{\mathrm{OE}}d'}{m}},$$

(17)

where b_1 and b_2 are uniform constants.

Proof. By Lemma 3 and the similar proving process in Lemma 5, we obtain that with the probability at least $1 - e^{-t} > 0$, for any $\gamma \geq 0$, $\rho \geq 0$ and $\mathbf{w}\in\mathcal{W}$, we have

$$\sup_{\mathrm{W}_c(D_{X'},D_{X_{\mathrm{A}}})\leq\rho}\mathbb{E}_{\mathbf{x}\sim D_{X'}}\ell_{\mathrm{OE}}(\mathbf{f_w};\mathbf{x})$$

$$\leq\gamma\rho + \frac{1}{m}\sum_{i=1}^{m}\phi_\gamma(\mathbf{w};\mathbf{x}_{\mathrm{A}}^i) + b_2 M_{\ell_{\mathrm{OE}}}\sqrt{\frac{t}{m}} + \gamma b_1\sqrt{\frac{\mathrm{diam}(\mathcal{W})L_{\mathrm{OE}}d'}{m}},$$

(18)

where b_1 and b_2 are uniform constants.

Let

$$\rho_m = \rho + b_1\sqrt{\frac{\mathrm{diam}(\mathcal{W})L_{\mathrm{OE}}d'}{m}},$$

and

$$\Delta_m = \sup_{\mathrm{W}_c(D_{X'},\widehat{D}_{X_{\mathrm{A}}})\leq\rho_m}\mathbb{E}_{\mathbf{x}\sim D_{X'}}\ell_{\mathrm{OE}}(\mathbf{f_w};\mathbf{x}) - \sup_{\mathrm{W}_c(D_{X'},\widehat{D}_{X_{\mathrm{A}}})\leq\rho}\mathbb{E}_{\mathbf{x}\sim D_{X'}}\ell_{\mathrm{OE}}(\mathbf{f_w};\mathbf{x}).$$

Note that

$$\inf_{\gamma\geq 0}\gamma\rho_m + \frac{1}{m}\sum_{i=1}^{m}\phi_\gamma(\mathbf{w};\mathbf{x}_{\mathrm{A}}^i) = \sup_{\mathrm{W}_c(D_{X'},\widehat{D}_{X_{\mathrm{A}}})\leq\rho_m}\mathbb{E}_{\mathbf{x}\sim D_{X'}}\ell_{\mathrm{OE}}(\mathbf{f_w};\mathbf{x}),$$

and by Lemma 6,

$$\Delta_m \leq L_c(\rho_m - \rho) = b_1 L_c\sqrt{\frac{\mathrm{diam}(\mathcal{W})L_{\mathrm{OE}}d'}{m}},$$

hence, by Eq. (18), we know that with the probability at least $1 - e^{-t} > 0$, for any $\rho \geq 0$ and $\mathbf{w} \in \mathcal{W}$,

$$\sup_{W_c(D_{X'}, D_{X_A}) \leq \rho} \mathbb{E}_{\mathbf{x} \sim D_{X'}} \ell_{\mathrm{OE}}(\mathbf{f_w}; \mathbf{x})$$

$$\leq \sup_{W_c(D_{X'}, \widehat{D}_{X_A}) \leq \rho} \mathbb{E}_{\mathbf{x} \sim D_{X'}} \ell_{\mathrm{OE}}(\mathbf{f_w}; \mathbf{x}) + b_1 L_c \sqrt{\frac{\mathrm{diam}(\mathcal{W}) L_{\mathrm{OE}} d'}{m}} + b_2 M_{\ell_{\mathrm{OE}}} \sqrt{\frac{t}{m}}, \tag{19}$$

where b_1 and b_2 are uniform constants.

Combining Lemma 3 with Eq. (19), we know that with the probability at least $1 - e^{-t} > 0$, for any $\rho > 0$ and $\mathbf{w} \in \mathcal{W}$,

$$\sup_{W_c(D_{X'}, D_{X_A}) \leq \rho} \mathbb{E}_{\mathbf{x} \sim D_{X'}} \ell_{\mathrm{OE}}(\mathbf{f_w}; \mathbf{x})$$

$$\leq \sup_{W_c(D_{X'}, \widehat{D}_{X_A}) \leq \rho} \mathbb{E}_{\mathbf{x} \sim D_{X'}} \ell_{\mathrm{OE}}(\mathbf{f_w}; \mathbf{x}) + b_2 M_{\ell_{\mathrm{OE}}} \sqrt{\frac{t}{m}} + b_1 \min\{L_c, \frac{M_{\ell_{\mathrm{OE}}}}{\rho}\} \sqrt{\frac{\mathrm{diam}(\mathcal{W}) L_{\mathrm{OE}} d'}{m}},$$

where b_1 and b_2 are uniform constants. $\qquad \square$

Lemma 8. *Given the same assumptions in Lemma 4, for a fixed $\mathbf{w}_0 \in \mathcal{W}$, then with the probability at least $1 - e^{-t} > 0$, for any $\rho \geq 0$*

$$\sup_{W_c(D_{X'}, \widehat{D}_{X_A}) \leq \rho} \mathbb{E}_{\mathbf{x} \sim D_{X'}} \ell_{\mathrm{OE}}(\mathbf{f}_{\mathbf{w}_0}; \mathbf{x}) \leq \sup_{W_c(D_{X'}, D_{X_A}) \leq \rho} \mathbb{E}_{\mathbf{x} \sim D_{X'}} \ell_{\mathrm{OE}}(\mathbf{f}_{\mathbf{w}_0}; \mathbf{x}) + 2 M_{\ell_{\mathrm{OE}}} \sqrt{\frac{2t}{m}}.$$

Proof of Lemma 8. By Sinha et al. (2018), it is clear that

$$\sup_{W_c(D_{X'}, D_{X_A}) \leq \rho} \mathbb{E}_{\mathbf{x} \sim D_{X'}} \ell_{\mathrm{OE}}(\mathbf{f}_{\mathbf{w}_0}; \mathbf{x}) = \inf_{\gamma \geq 0} [\gamma \rho + \mathbb{E}_{\mathbf{x} \sim D_{X_A}} \phi_\gamma(\mathbf{w}_0; \mathbf{x})]$$

Therefore, for each $\epsilon > 0$, there exists a constant $\gamma_\epsilon \geq 0$ such that

$$\gamma_\epsilon \rho + \mathbb{E}_{\mathbf{x} \sim D_{X_A}} \phi_{\gamma_\epsilon}(\mathbf{w}_0; \mathbf{x}) \leq \sup_{W_c(D_{X'}, D_{X_A}) \leq \rho} \mathbb{E}_{\mathbf{x} \sim D_{X'}} \ell_{\mathrm{OE}}(\mathbf{f}_{\mathbf{w}_0}; \mathbf{x}) + \epsilon.$$

Combining the above inequality, Lemma 2 and McDiarmid's Inequality, then with the probability at least

$$1 - \exp\left(\frac{-\epsilon_0^2 m}{2 M_{\ell_{\mathrm{OE}}}^2}\right) > 0,$$

we have

$$\mathbb{E}_{\mathbf{x} \sim \widehat{D}_{X_A}} \phi_{\gamma_\epsilon}(\mathbf{w}_0; \mathbf{x}) \leq \mathbb{E}_{\mathbf{x} \sim D_{X_A}} \phi_{\gamma_\epsilon}(\mathbf{w}_0; \mathbf{x}) + \epsilon_0.$$

If we set $t = \epsilon_0^2 m / 2 M_{\ell_{\mathrm{OE}}}^2$, then

$$\epsilon_0 = M_{\ell_{\mathrm{OE}}} \sqrt{\frac{2t}{m}}.$$

Hence, with the probability at least $1 - e^{-t} > 0$, we have

$$\gamma_\epsilon \rho + \mathbb{E}_{\mathbf{x} \sim \widehat{D}_{X_A}} \phi_{\gamma_\epsilon}(\mathbf{w}_0; \mathbf{x}) \leq \sup_{W_c(D_{X'}, D_{X_A}) \leq \rho} \mathbb{E}_{\mathbf{x} \sim D_{X'}} \ell_{\mathrm{OE}}(\mathbf{f}_{\mathbf{w}_0}; \mathbf{x}) + \epsilon + M_{\ell_{\mathrm{OE}}} \sqrt{\frac{2t}{m}},$$

which implies that with the probability at least $1 - e^{-t} > 0$,

$$\sup_{W_c(D_{X'}, \widehat{D}_{X_A}) \leq \rho} \mathbb{E}_{\mathbf{x} \sim D_{X'}} \ell_{\mathrm{OE}}(\mathbf{f}_{\mathbf{w}_0}; \mathbf{x}) \leq \sup_{W_c(D_{X'}, D_{X_A}) \leq \rho} \mathbb{E}_{\mathbf{x} \sim D_{X'}} \ell_{\mathrm{OE}}(\mathbf{f}_{\mathbf{w}_0}; \mathbf{x}) + \epsilon + M_{\ell_{\mathrm{OE}}} \sqrt{\frac{2t}{m}},$$

because

$$\gamma_\epsilon \rho + \mathbb{E}_{\mathbf{x} \sim \widehat{D}_{X_A}} \phi_{\gamma_\epsilon}(\mathbf{w}_0; \mathbf{x}) \geq \sup_{W_c(D_{X'}, \widehat{D}_{X_A}) \leq \rho} \mathbb{E}_{\mathbf{x} \sim D_{X'}} \ell_{\mathrm{OE}}(\mathbf{f}_{\mathbf{w}_0}; \mathbf{x}).$$

By setting $\epsilon = M_{\ell_{\mathrm{OE}}} \sqrt{2t/m}$, we complete this proof. $\qquad \square$

Lemma 9. *If $0 \le \ell(\mathbf{f_w}; \mathbf{x}, y) \le M_\ell$, then with the probability at least $1 - e^{-t} > 0$, we have that for any $\mathbf{w} \in \mathcal{W}$,*

$$\mathbb{E}_{(\mathbf{x},y)\sim D_{X_I Y_I}} \ell(\mathbf{f_w}; \mathbf{x}, y) - \frac{1}{n}\sum_{i=1}^{n} \ell(\mathbf{f_w}; \mathbf{x}_I^i, y_I^i) \le \frac{b_0 M_\ell}{\sqrt{n}}\int_0^1 \sqrt{\log \mathcal{N}(\mathcal{F}, M_\ell \epsilon, L^\infty)}\mathrm{d}\epsilon + M_\ell\sqrt{\frac{2t}{n}},$$

where b_0 is a uniform constant.

Proof of Lemma 9. Let

$$X_{\ell(\mathbf{f_w};\cdot)} = \mathbb{E}_{(\mathbf{x},y)\sim D_{X_I Y_I}} \ell(\mathbf{f_w}; \mathbf{x}, y) - \frac{1}{n}\sum_{i=1}^{n} \ell(\mathbf{f_w}; \mathbf{x}_I^i, y_I^i).$$

Then, it is clear that

$$\mathbb{E}_{S\sim D_{X_I Y_I}^n} X_{\ell(\mathbf{f_w};\cdot)} = 0.$$

By Proposition 2.6.1 and Lemma 2.6.8 in Vershynin (2018),

$$\|X_{\ell(\mathbf{f_w};\cdot)} - X_{\ell(\mathbf{f_{w'}};\cdot)}\|_{\Phi_2} \le \frac{c_0}{\sqrt{n}}\|\ell(\mathbf{f_w};\cdot) - \ell(\mathbf{f_{w'}};\cdot)\|_{L^\infty},$$

where $\|\cdot\|_{\Phi_2}$ is the sub-gaussian norm and c_0 is a uniform constant. Therefore, by Dudley's entropy integral (Vershynin, 2018), we have

$$\mathbb{E}_{S\sim D_{X_I Y_I}^n} \sup_{\mathbf{w}\in\mathcal{W}} X_{\ell(\mathbf{f_w};\cdot)} \le \frac{b_0}{\sqrt{n}}\int_0^{+\infty} \sqrt{\log \mathcal{N}(\mathcal{F}, \epsilon, L^\infty)}\mathrm{d}\epsilon,$$

where b_0 is a uniform constant and

$$\mathcal{F} = \{\ell(\mathbf{f_w}; \mathbf{x}, y) : \mathbf{w} \in \mathcal{W}\}.$$

Note that

$$
\begin{aligned}
\mathbb{E}_{S\sim D_{X_I Y_I}^n} \sup_{\mathbf{w}\in\mathcal{W}} X_{\ell(\mathbf{f_w};\cdot)} &\le \frac{b_0}{\sqrt{n}}\int_0^{+\infty} \sqrt{\log \mathcal{N}(\mathcal{F}, \epsilon, L^\infty)}\mathrm{d}\epsilon \\
&= \frac{b_0}{\sqrt{n}}\int_0^{M_\ell} \sqrt{\log \mathcal{N}(\mathcal{F}, \epsilon, L^\infty)}\mathrm{d}\epsilon \\
&= \frac{b_0}{\sqrt{n}}M_\ell\int_0^1 \sqrt{\log \mathcal{N}(\mathcal{F}, M_\ell \epsilon, L^\infty)}\mathrm{d}\epsilon.
\end{aligned}
$$

Then, similar to the proof of Lemma 8, we use McDiarmid's Inequality, then with the probability at least $1 - e^{-t} > 0$, for any $\mathbf{w} \in \mathcal{W}$,

$$X_{\ell(\mathbf{f_w};\cdot)} \le \frac{b_0}{\sqrt{n}}M_\ell\int_0^1 \sqrt{\log \mathcal{N}(\mathcal{F}, M_\ell \epsilon, L^\infty)}\mathrm{d}\epsilon + M_\ell\sqrt{\frac{2t}{n}}.$$

$\square$

Lemma 10. *If $0 \le \ell(\mathbf{f_w}; \mathbf{x}, y) \le M_\ell$, then for a fixed $\mathbf{w}_0 \in \mathcal{W}$, with the probability at least $1 - e^{-t} > 0$,*

$$\frac{1}{n}\sum_{i=1}^{n} \ell(\mathbf{f_{w_0}}; \mathbf{x}_I^i, y_I^i) - \mathbb{E}_{(\mathbf{x},y)\sim D_{X_I Y_I}} \ell(\mathbf{f_{w_0}}; \mathbf{x}, y) \le M_\ell\sqrt{\frac{2t}{n}}.$$

Proof of Lemma 10. Similar to the proof of Lemma 8, McDiarmid's Inequality implies this result.
$\square$

Lemma 11. *If*

- $0 \le \ell(\mathbf{f_w}; \mathbf{x}, y) \le M_\ell$,
- *$\ell(\mathbf{f_w}; \mathbf{x}, y)$ is L-Lipschitz w.r.t. norm $\|\cdot\|$, i.e., for any $(\mathbf{x}, y) \in \mathcal{X} \times \mathcal{Y}$, and $\mathbf{w}, \mathbf{w}' \in \mathcal{W}$,*

$$|\ell(\mathbf{f_w}; \mathbf{x}, y) - \ell(\mathbf{f_{w'}}; \mathbf{x}, y)| \le L\|\mathbf{w} - \mathbf{w}'\|,$$

- *the parameter space $\mathcal{W} \subset \mathbb{R}^{d'}$ satisfies that*

$$\mathrm{diam}(\mathcal{W}) = \sup_{\mathbf{w}, \mathbf{w}' \in \mathcal{W}} \|\mathbf{w} - \mathbf{w}'\| < +\infty,$$

then with the probability at least $1 - e^{-t} > 0$, we have that for any $\mathbf{w} \in \mathcal{W}$,

$$\mathbb{E}_{(\mathbf{x}, y) \sim D_{X_\mathrm{I} Y_\mathrm{I}}} \ell(\mathbf{w}; \mathbf{x}, y) - \frac{1}{n} \sum_{i=1}^{n} \ell(\mathbf{w}; \mathbf{x}_\mathrm{I}^i, y_\mathrm{I}^i) \leq b_0 \sqrt{\frac{M_\ell \mathrm{diam}(\mathcal{W}) L d'}{n}} + M_\ell \sqrt{\frac{2t}{n}},$$

where b_0 is a uniform constant.

Proof of Lemma 11. The proof is similar to Corollary 1 in Sinha et al. (2018) and Lemma 5. Note that

$$\mathcal{F} = \{\ell(\mathbf{f}_{\mathbf{w}}; \mathbf{x}, y) : \mathbf{w} \in \mathcal{W}\},$$

and $\ell(\mathbf{f}_{\mathbf{w}}; \mathbf{x}, y)$ is L-Lipschitz w.r.t. norm $\|\cdot\|$, therefore,

$$\mathcal{N}(\mathcal{F}, M_\ell \epsilon, L^\infty) \leq \mathcal{N}(\mathcal{W}, M_\ell \epsilon / L, \|\cdot\|) \leq (1 + \frac{\mathrm{diam}(\mathcal{W}) L}{M_\ell \epsilon})^{d'},$$

which implies that

$$\int_0^1 \sqrt{\log(\mathcal{N}(\mathcal{F}, M_\ell \epsilon, L^\infty)} \mathrm{d}\epsilon \leq \sqrt{d'} \int_0^1 \sqrt{\log(1 + \frac{\mathrm{diam}(\mathcal{W}) L}{M_\ell \epsilon})} \mathrm{d}\epsilon$$

$$\leq \sqrt{d'} \int_0^1 \sqrt{\frac{\mathrm{diam}(\mathcal{W}) L}{M_\ell \epsilon}} \mathrm{d}\epsilon = 2 \sqrt{\frac{\mathrm{diam}(\mathcal{W}) L d'}{M_\ell}}.$$

By Lemma 9, we obtain this result. $\qquad\square$

E Further Discussions

As discussed in Section 4.2, we realize the dual optimization objective following Eq. (9), searching for the worst OOD data in a finite-dimensional space to ease the computation. Furthermore, directly searching in the input space is typically hard for optimization (Madry et al., 2018; Wang et al., 2021b), where the results can easily stuck at sub-optimal solutions and the computation is time-consuming. Therefore, we suggest perturbing the worst OOD data in the embedding space. Denote the embedding features of an input by $\mathbf{e}(\mathbf{x})$, we consider the bi-level optimization problem:

$$\inf_{\gamma \geq 0} \Big\{ \gamma \rho + \frac{1}{m} \sum_{i=1}^{m} \phi_\gamma(\mathbf{w}; \mathbf{e}(\mathbf{x}_A^i)) \Big\},$$

$$\text{where } \phi_\gamma(\mathbf{w}; \mathbf{e}(\mathbf{x}_A^i)) = \sup_{\mathbf{p}^i \in \mathcal{E}} \big\{ \ell_{\mathrm{OE}}(\mathbf{h}(\mathbf{e}(\mathbf{x}_A^i) + \mathbf{p}^i); \mathbf{e}(\mathbf{x}_A^i)) - \gamma \|\mathbf{p}^i\|_1 \big\}.$$

Such an bi-level problem can be solved by alternative optimization (Huang et al., 2023b; Liu et al., 2021): we first find the proper value of $\mathbf{p}^i$ that approaches to the true value of $\phi_\gamma(\mathbf{w}; \mathbf{e}(\mathbf{x}_A^i))$, and then we update the value of γ that leads to the smallest value of $\gamma \rho + \frac{1}{m} \sum_{i=1}^{m} \phi_\gamma(\mathbf{w}; \mathbf{e}(\mathbf{x}_A^i))$. The gradient descent/ascent can be adopted for optimization. Specifically, for the perturbation $\mathbf{p}^i$, each optimization step is

$$\phi_\gamma(\mathbf{w}; \mathbf{e}(\mathbf{x}_A^i)) \leftarrow \ell_{\mathrm{OE}}\big(\mathbf{h}(\mathbf{e}(\mathbf{x}_A^i) + \mathbf{p}^i); \mathbf{e}(\mathbf{x}_A^i)\big) - \gamma \big\|\mathbf{p}^i\big\|_1,$$

$$\mathbf{p}^i \leftarrow \mathbf{p}^i + \mathrm{ps} \nabla_{\mathbf{p}^i} \phi_\gamma(\mathbf{w}; \mathbf{e}(\mathbf{x}_A^i)),$$

where ps is the learning rate. For γ, the optimization step follows:

$$\gamma \leftarrow \gamma - \beta \Big\{ \rho - \frac{1}{m} \sum_{i=1}^{m} \big\|\mathbf{p}^i\big\|_1 \Big\},$$

with β the learning rate. Furthermore, to avoid the extreme value and/or the negative value of γ, we should conduct value clipping for γ, which is given by

$$\gamma \leftarrow \min(\max(\gamma, \gamma_{\max}), 0),$$

where we constrain the minimum of γ to be 0 and the maximum of γ to be $\gamma_{\max}$.

E.1 Understanding Theoretical Results

Theorem 2 justifies that when the model complexity and the sample size are large enough, the empirical solution given by our DAL risk will converge to its optimal value, i.e., $\min_{\mathbf{w}} R_D(\mathbf{w}; \rho)$. Therefore, the difference between the expected and the empirical error is bounded w.r.t. the DAL risk. Theorem 3 goes one step further, studying the detection risk w.r.t. (unseen) real OOD data. It states that the open-world performance of our DAL depends on both the approximate risk and the estimation error. The former models the best performance (i.e., Bayes optimal) that our DAL can achieve, and the latter depends on the OOD distribution gap, the radius, and the excess error introduced in Theorem 2. In summary, Theorem 2 considers the convergence for DAL itself, while Theorem 3 justifies that DAL can mitigate the OOD distribution discrepancy in the open world.

E.2 Comparison with DOE

A parallel work, named DOE (Wang et al., 2023), also focuses on mitigating the OOD distribution discrepancy issue. Overall, they state that model perturbation can lead to input transformation, and thus learning from the perturbed model can make the predictor learn from diverse distributions with respect to auxiliary OOD cases. Moreover, to make the transformed data benefit the model most, DOE searches for the associated perturbation that leads to the worst OOD regret.

Similar to DOE, we also learn from the worst OOD cases to mitigate the distribution discrepancy, but DAL further enjoys the following two strengths. 1) From the theoretical perspective, our clear definition of the candidate OOD distribution space, i.e., the Wasserstein ball, allows us to investigate the impact of DAL for open-world OOD detection (cf., Theorem 3). In contrast, DOE only constrains the magnitude of the perturbation strength, making it limited to proving convergence w.r.t. their

Table 4: ID accuracy on the CIFAR benchmarks for those methods that require model training.

Method	ERM	CSI	VOS	OE	Energy-OE	ATOM	DOE	POEM	DAL
CIFAR-10	94.28	94.33	94.58	95.22	94.84	95.12	94.28	93.32	95.01
CIFAR-100	73.98	74.30	75.50	75.90	71.61	74.04	74.51	74.85	76.13

proposed learning objective (cf., Theorem 2 in Wang et al. (2023)). 2) From the algorithmic perspective, we directly search for the worst OOD data in the embedding space, more effective than DAL, which requires searching the model perturbation for the whole model. As a result, our theoretically-driven framework, i,e, DAL, yields superior performance over DOE in Table 1 while requiring less computation cost (DAL take only half the training time compared with DOE per epoch).

E.3 Discussing about Limitations

In theory, our main drawback lies in the trade-off between estimation and approximation errors (cf., Theorem 3), where we may not get a very tight bound for the real OOD risk. In algorithm, the worst OOD data are constrained in the ball around the auxiliary OOD data (cf., Algorithm 1), of which the coverage may not include real OOD data. Moreover, we conduct distribution augmentation in the embedding space, where our Theorem 3 can only be applied. Other data generation approaches, which can lead to more complex forms of distribution augmentation in the input space, are also of interest. Our future studies will focus on advanced learning schemes that address the above issues, e.g., modeling the data generation process through the causality perspective (Zhang et al., 2022).

F Further Evaluations

We provide more information about evaluation setups and conduct additional experiments on DAL.

F.1 Hardware Configurations

All experiments are realized by Pytorch 1.81 with CUDA 11.1, using machines equipped with GeForce RTX 3090 GPUs and AMD Threadripper 3960X Processors.

F.2 ID Accuracy

We report the ID accuracy for those methods that require model training on the CIFAR benchmarks, of which the results are summarized in Table 4. We also list the results for the model conventionally trained on ID data with empirical risk minimization (ERM). Overall, most of the considered methods can preserve relatively high ID accuracy. Moreover, those methods that regularize predictors by auxiliary OOD data, such as OE and DAL, can even show further improvements. It indicates that learning with auxiliary data can achieve high detection performance and maintain good ID accuracy.

F.3 Other Scoring Functions

We further claim that many advanced scoring strategies other than MSP can also benefit from DAL. In Table 5, we compare the OOD detection performance before (w/o train) and after (w/ DAL) DAL training across a set of representative scoring strategies, including MSP, Fee Energy, ASH, Mahalanobis, and KNN. We also compare the results after OE training (w/ OE). As we can see, both OE and DAL can lead to much better results than before training, and DAL can further boost detection performance over OE. It indicates that the benefits of our proposal are not limited to the specific scoring function of MSP. However, Mahalanobis fails (FPR95 more than 95) on CIFAR-100 after OE and DAL training, which may require further exploration.

F.4 Mean and Standard Deviation

This section validates the experiments on CIFAR benchmarks with five individual trials (random seeds), comparing between our DAL and OE. Besides the individual results, we also summarize the mean performance and standard deviation across the trails for both CIFAR-10 and CIFAR-100. We

Table 5: Comparison on the CIFAR benchmarks with different scoring strategies.

	MSP		Free Energy		ASH		Mahalanobis		KNN	
	FPR	AUROC	FPR	AUROC	FPR	AUROC	FPR	AUROC	FPR	AUROC
CIFAR-10										
w/o train	50.15	91.02	33.21	91.01	32.98	91.85	46.64	88.59	33.38	93.76
w/ OE	4.67	98.88	3.40	98.98	3.35	98.99	15.80	94.32	5.50	98.71
w/ DAL	2.68	99.01	2.59	98.99	2.50	98.70	12.75	95.55	5.04	97.58
CIFAR-100										
w/o train	78.61	75.95	69.84	75.20	59.31	84.46	72.37	82.70	59.31	84.46
w/ OE	43.14	90.27	36.98	92.66	33.82	93.36	-	-	53.14	83.50
w/ DAL	29.68	93.92	29.63	93.83	29.73	94.05	-	-	50.46	84.75

Table 6: Comparison of DAL and outlier exposure on CIFAR-10 with 5 individual trails. ↓ (or ↑) indicates smaller (or larger) values are preferred; and a bold font indicates the best results in the corresponding column.

Trails	SVHN		LSUN		iSUN		Textures		Places365		Average	
	FPR95 ↓	AUROC ↑	FPR95 ↓	AUROC ↑	FPR95 ↓	AUROC ↑	FPR95 ↓	AUROC ↑	FPR95 ↓	AUROC ↑	FPR95 ↓	AUROC ↑
OE												
#1	1.50	99.23	1.10	99.33	1.70	99.18	4.00	98.64	11.30	97.09	3.92	98.69
#2	1.25	99.15	1.05	99.49	2.20	98.88	4.15	98.59	11.60	97.08	4.05	98.63
#3	1.25	99.38	1.05	99.42	1.75	99.01	4.00	98.82	11.10	97.04	3.83	98.73
#4	1.70	99.13	1.05	99.52	2.10	99.12	4.20	98.55	11.65	97.08	4.14	98.68
#5	1.35	99.17	1.30	99.49	1.40	99.26	4.60	99.00	11.75	97.03	1.08	98.79
mean	1.41	99.21	1.10	99.45	1.83	99.09	4.19	98.72	11.48	97.06	3.40	98.70
± std	± 0.17	± 0.10	± 0.02	± 0.07	± 0.28	± 0.15	± 0.22	± 0.18	± 0.24	± 0.03	± 1.16	± 0.05
DAL												
#1	0.80	99.84	0.40	99.59	0.95	99.29	2.65	98.85	7.75	97.37	2.51	98.86
#2	0.90	99.24	0.60	99.57	1.20	99.26	2.65	98.84	8.15	97.43	2.70	98.87
#3	0.90	99.16	0.65	99.52	1.15	99.14	2.40	98.75	8.20	97.35	2.66	98.78
#4	0.80	99.37	0.55	99.63	0.95	99.34	2.85	98.89	7.95	97.39	2.62	98.93
#5	1.25	99.39	0.40	99.61	0.85	99.39	2.75	98.90	7.70	97.46	2.59	98.95
mean	**0.93**	**99.40**	**0.52**	**99.58**	**1.02**	**99.28**	**2.65**	**98.84**	**7.95**	**97.40**	**2.61**	**98.87**
± std	**± 0.17**	**± 0.24**	**± 0.10**	**± 0.04**	**± 0.13**	**± 0.08**	**± 0.15**	**± 0.05**	**± 0.20**	**± 0.04**	**± 0.06**	**± 0.06**

summarize the experimental results in Tables 6-7. As we can see, our DAL can not only lead to improved performance in OOD detection, but our performance is also very stable across different choices of ID datasets and real OOD datasets.

F.5 Effects of Hyper-parameters

We further test the impacts of other hyper-parameters on the performance in OOD detection, where we consider γ_{max}, β, `num_search`, and `ps` on CIFAR benchmarks.

Impacts of γ. The exact values of γ are dynamically determined by γ_{max}, ρ, β, and the current model $\mathbf{f_w}$. To evaluation the effects of γ, we conduct experiments on CIFAR benchmarks with different γ_{max}, ρ, and β, of which the results are summarized in Table 8-9. Overall, our method is pretty robust to different choices of hyper-parameters, in that the results for most of the hyper-parameter setups can lead to promising improvement over the original outlier exposure. Specifically, for γ_{max}, most of its different choices can lead to effective OOD detection with the proper choices of ρ and β, but its values should not be too small (e.g., $\gamma_{max} = 0.1$). The reason is that if the value of γ is too small, the distance between the worst-cases OOD features, i.e., $\mathbf{g_w}(\mathbf{x}) + \mathbf{p}$, and the original OOD features, i.e., $\mathbf{g_w}(\mathbf{x})$, can be very long, occupying the regions that should belong to ID data. It will make the model confused between ID and OOD cases and thus lead to unsatisfactory results. A similar conclusion can also be applied for β: when its value is too large (such as $\beta = 5$), values of $\mathbf{g_w}(\mathbf{x}) + \mathbf{p}$ can also be arbitrarily large, making the current model hardly learn to discern ID and OOD patterns.

Impacts of `num_search` and `ps`. We also provides the results on CIFAR benchmarks with different `num_search` and `ps`, and the results can be found in Tables 10-11. As we can see, even with some extreme values, such as `num_search` = 500 and `ps` = 100, the resultant models still enjoy the improvements over outlier exposure, indicating that our method is pretty robust to these hyper-parameters. The reason is that our proper selection of ρ will constrain the resultant perturbation to be beneficial, avoiding the worst OOD distribution to not intrude the region that belongs to ID data.

Table 7: Comparison of DAL and outlier exposure on CIFAR-100 with 5 individual trails. ↓ (or ↑) indicates smaller (or larger) values are preferred, and a bold font indicates the best results in the corresponding column.

Trails	SVHN FPR95↓	SVHN AUROC↑	LSUN FPR95↓	LSUN AUROC↑	iSUN FPR95↓	iSUN AUROC↑	Textures FPR95↓	Textures AUROC↑	Places365 FPR95↓	Places365 AUROC↑	Average FPR95↓	Average AUROC↑
						OE						
#1	44.45	91.76	15.75	97.26	45.95	88.80	47.35	89.80	54.10	87.90	41.52	91.10
#2	42.75	91.93	15.85	97.22	46.85	88.91	46.75	89.78	53.05	88.04	41.05	91.18
#3	43.75	91.88	15.95	97.34	52.25	87.62	47.15	89.49	54.10	88.03	42.64	90.87
#4	41.30	92.23	16.15	97.27	46.90	88.76	47.00	89.73	54.40	87.91	41.15	91.18
#5	42.55	91.92	16.20	97.22	44.70	89.66	47.35	89.47	54.35	87.82	41.03	91.22
mean	42.96	91.94	15.97	97.26	47.33	88.75	47.12	89.65	54.00	87.94	41.47	91.10
± std	± 1.07	± 0.15	± 0.17	± 0.04	± 2.58	± 0.65	± 0.23	± 0.14	± 0.49	± 0.08	± 0.61	± 0.13
						DAL						
#1	19.35	96.21	16.05	96.78	26.05	94.23	37.60	91.57	49.35	88.81	29.68	93.52
#2	22.65	95.55	16.30	96.73	26.35	94.23	36.20	91.91	48.50	88.74	30.00	93.43
#3	20.15	96.15	16.20	96.91	29.85	93.55	37.85	91.60	47.90	88.95	30.39	93.43
#4	14.50	96.72	16.75	96.58	33.75	92.68	37.60	91.63	49.70	88.80	30.46	93.28
#5	22.70	95.90	15.20	96.91	27.15	94.58	37.00	91.82	49.65	88.73	30.34	93.59
mean	**19.87**	**96.11**	**16.10**	**96.78**	**28.63**	**93.85**	**37.25**	**91.70**	**49.01**	**88.80**	**30.17**	**93.45**
± std	± 2.99	± 0.39	± 0.51	± 0.12	± 2.89	± 0.68	± 0.60	± 0.13	± 0.71	± 0.08	± 0.29	± 0.10

Table 8: Detection Performance on CIFAR-10 dataset with different choices of β, ρ, and γ_{max}, where we report the FPR95 / AUROC for each individual trail setup.

$\gamma_{max}=50$

β \ ρ	1e-2	1e-1	1	10	100
1e-3	2.95 / 99.07	2.80 / **99.07**	2.96 / 99.02	2.80 / 98.31	91.85 / 64.43
5e-3	2.95 / 99.01	3.05 / 99.00	2.97 / 99.04	2.69 / 98.16	92.79 / 55.39
1e-2	2.79 / 98.95	**2.68** / 99.05	2.84 / 98.88	2.71 / 98.67	96.48 / 44.97
5e-2	3.08 / 98.98	3.03 / 98.98	2.85 / 98.98	2.88 / 98.79	95.58 / 45.79
1e-1	2.79 / 98.96	2.98 / 98.99	2.75 / 99.02	10.22 / 96.37	88.96 / 72.68
5e-1	2.82 / 99.00	2.95 / 99.01	2.81 / 99.05	4.34 / 96.58	95.51 / 46.60
1	2.94 / 98.93	2.88 / 99.02	3.19 / 99.00	52.76 / 94.36	95.05 / 53.89
5	2.98 / 98.91	2.77 / 98.96	3.00 / 99.06	94.44 / 62.90	95.57 / 52.51

$\gamma_{max}=10$

β \ ρ	1e-2	1e-1	1	10	100
1e-3	3.06 / 99.05	2.82 / 99.06	2.84 / 98.97	**2.41** / 97.95	94.65 / 46.60
5e-3	2.85 / 99.00	2.80 / **99.09**	2.93 / 99.04	2.56 / 98.21	94.69 / 57.61
1e-2	2.91 / 98.98	2.98 / 99.04	2.56 / 99.02	2.58 / 98.28	95.48 / 50.70
5e-2	2.94 / 99.01	2.91 / 99.00	2.71 / 99.03	2.81 / 98.53	97.80 / 43.86
1e-1	3.02 / 99.04	2.77 / 99.04	2.87 / 99.02	14.11 / 95.47	96.00 / 55.75
5e-1	2.90 / 98.98	2.89 / 99.04	2.73 / 99.06	67.48 / 90.50	94.64 / 56.57
1	2.81 / 98.96	2.89 / 99.04	2.82 / 99.04	90.97 / 70.65	87.12 / 56.72
5	2.73 / 98.98	2.90 / 99.03	14.04 / 95.64	93.01 / 45.50	88.61 / 69.65

$\gamma_{max}=5$

β \ ρ	1e-2	1e-1	1	10	100
1e-3	3.05 / 99.04	2.84 / 98.98	2.81 / 98.99	2.79 / 98.20	93.77 / 64.09
5e-3	2.82 / 99.02	2.85 / **99.20**	2.97 / 99.00	2.76 / 98.37	93.50 / 63.44
1e-2	2.82 / 98.99	2.95 / 99.02	2.93 / 99.03	2.68 / 98.48	94.42 / 52.51
5e-2	2.99 / 98.98	2.81 / 98.99	2.87 / 98.91	5.21 / 95.95	87.32 / 71.25
1e-1	2.91 / 98.95	2.70 / 99.06	2.90 / 99.03	3.84 / 96.46	95.17 / 57.61
5e-1	3.03 / 99.01	3.06 / 99.00	**2.75** / 99.02	88.76 / 69.56	94.68 / 41.66
1	2.67 / 99.00	2.86 / 99.03	2.94 / 99.00	97.40 / 45.45	95.03 / 48.58
5	2.87 / 98.93	2.82 / 98.97	63.22 / 87.13	98.97 / 58.50	95.49 / 50.51

$\gamma_{max}=1$

β \ ρ	1e-2	1e-1	1	10	100
1e-3	2.74 / 98.92	**2.62** / 98.95	2.64 / 98.93	2.70 / 98.93	92.36 / 57.40
5e-3	2.64 / 99.00	2.78 / 98.98	2.86 / 98.82	2.68 / 98.16	94.72 / 58.59
1e-2	2.69 / 99.02	2.69 / 99.00	2.69 / 98.97	2.79 / 98.19	93.39 / 57.55
5e-2	2.67 / 98.94	2.75 / 98.93	2.71 / 98.97	2.74 / 98.64	94.60 / 52.14
1e-1	2.91 / 98.95	2.70 / 99.06	2.71 / **99.07**	22.93 / 94.15	92.55 / 67.68
5e-1	2.66 / 98.99	2.64 / 98.99	2.90 / 98.87	79.75 / 89.56	93.76 / 55.94
1	2.78 / 99.01	2.98 / 98.94	2.56 / 98.96	52.66 / 90.50	92.57 / 90.03
5	2.68 / 99.03	2.68 / 98.96	2.69 / 98.96	25.31 / 94.53	97.42 / 43.10

$\gamma_{max}=0.5$

β \ ρ	1e-2	1e-1	1	10	100
1e-3	2.90 / 98.99	2.74 / 98.89	2.74 / 98.87	2.56 / 98.20	94.75 / 65.65
5e-3	2.64 / 98.94	2.79 / 98.89	2.53 / 98.81	2.54 / 98.32	97.22 / 41.88
1e-2	2.65 / 98.93	2.74 / 98.94	2.78 / 98.85	2.70 / 98.50	94.86 / 56.57
5e-2	2.68 / **98.98**	2.73 / 98.95	2.89 / 98.80	3.50 / 96.78	92.13 / 65.63
1e-1	2.68 / 98.94	2.63 / 98.91	2.89 / 98.86	11.31 / 96.11	91.44 / 70.20
5e-1	3.07 / 98.89	2.74 / 98.89	**2.50** / 98.68	18.10 / 95.47	93.15 / 59.78
1	2.82 / 98.85	2.61 / 98.89	2.76 / 98.81	12.58 / 95.80	94.61 / 61.49
5	2.61 / 98.84	2.73 / 98.92	2.74 / 98.73	83.18 / 90.90	94.14 / 60.82

$\gamma_{max}=0.1$

β \ ρ	1e-2	1e-1	1	10	100
1e-3	2.75 / **98.59**	53.32 / 94.12	82.19 / 92.03	2.52 / 98.41	95.24 / 51.41
5e-3	2.83 / 98.55	**2.46** / 98.55	91.80 / 59.84	90.23 / 70.99	95.65 / 69.73
1e-2	2.47 / 98.48	2.56 / 98.55	87.64 / 88.24	97.56 / 71.35	88.87 / 77.29
5e-2	91.10 / 91.70	**2.46** / 98.53	87.24 / 90.28	90.04 / 81.11	96.49 / 44.84
1e-1	87.87 / 91.66	3.00 / 95.54	86.08 / 71.34	89.70 / 72.59	73.47 / 79.13
5e-1	90.51 / 84.74	92.42 / 92.06	91.78 / 90.73	89.48 / 81.07	94.27 / 59.21
1	93.82 / 89.51	92.29 / 90.44	96.46 / 83.90	79.04 / 86.78	94.06 / 50.42
5	80.22 / 91.03	87.43 / 89.21	91.98 / 59.04	91.55 / 63.98	94.18 / 61.55

Table 9: Detection Performance on CIFAR-100 dataset with different choices of β, ρ, and $\gamma_{\max}$, where we report the FPR95 / AUROC for each individual trail setup.

$\gamma_{\max}=50$

β	ρ = 1e-2	1e-1	1	10	100
1e-3	31.72 / 93.37	30.84 / 93.51	31.50 / 93.27	31.08 / 92.47	87.70 / 86.84
5e-3	33.36 / 92.70	30.23 / 93.61	31.27 / 93.32	29.98 / 92.94	96.98 / 36.34
1e-2	31.73 / 93.32	35.42 / 92.42	30.86 / 93.61	31.22 / 92.34	87.17 / 86.80
5e-2	33.69 / 92.66	32.50 / 93.18	31.29 / 93.40	30.92 / 92.68	87.23 / 86.57
1e-1	32.21 / 93.18	32.42 / 93.31	33.77 / 92.98	29.48 / 93.04	87.14 / 87.27
5e-1	33.44 / 93.16	36.19 / 92.71	33.55 / 92.85	34.83 / 91.70	86.91 / 87.22
1	33.01 / 93.16	33.80 / 92.64	**28.99 / 93.87**	36.22 / 91.41	92.34 / 52.72
5	34.62 / 92.55	32.90 / 93.15	36.00 / 92.14	95.59 / 89.09	93.69 / 96.87

$\gamma_{\max}=10$

β	ρ = 1e-2	1e-1	1	10	100
1e-3	33.07 / 92.92	33.93 / 92.85	35.09 / 92.44	30.39 / 92.59	94.25 / 48.00
5e-3	34.03 / 92.81	33.64 / 92.88	30.43 / 93.66	33.75 / 92.00	96.58 / 48.51
1e-2	35.80 / 92.46	33.40 / 93.16	34.52 / 92.90	32.02 / 91.76	88.11 / 86.65
5e-2	33.38 / 93.19	32.95 / 93.29	29.74 / **93.63**	29.13 / 92.71	95.18 / 50.19
1e-1	31.77 / 93.33	31.94 / 93.31	35.34 / 92.78	**27.80** / 93.02	95.48 / 56.81
5e-1	34.12 / 92.71	35.26 / 92.86	31.71 / 93.23	79.79 / 89.56	89.26 / 86.60
1	32.90 / 93.05	34.13 / 92.86	31.64 / 93.05	47.37 / 91.31	96.10 / 46.88
5	32.65 / 93.13	34.41 / 92.86	33.02 / 91.80	57.19 / 90.72	89.12 / 87.75

$\gamma_{\max}=5$

β	ρ = 1e-2	1e-1	1	10	100
1e-3	33.58 / 92.84	34.61 / 92.35	32.90 / 92.91	30.55 / 92.66	95.80 / 54.59
5e-3	33.80 / 92.87	34.98 / 92.61	31.87 / 93.39	27.36 / 93.18	89.37 / 51.52
1e-2	36.96 / 92.48	34.87 / 93.01	30.87 / 93.01	31.75 / 92.82	85.67 / 88.23
5e-2	36.00 / 92.49	32.10 / 93.24	31.31 / **93.55**	30.70 / 92.95	85.80 / 86.38
1e-1	33.64 / 92.75	31.82 / 93.09	32.55 / 92.97	32.42 / 92.22	91.16 / 84.87
5e-1	34.03 / 92.69	33.03 / 93.09	32.99 / 93.19	81.64 / 89.24	89.67 / 87.08
1	34.85 / 92.61	32.73 / 93.31	29.53 / 93.74	63.16 / 90.50	87.71 / 87.06
5	34.59 / 92.69	33.14 / 93.16	72.10 / 90.79	40.65 / 91.30	89.45 / 86.70

$\gamma_{\max}=1$

β	ρ = 1e-2	1e-1	1	10	100
1e-3	37.24 / 91.87	30.42 / 93.44	33.45 / 92.88	30.17 / 92.77	95.60 / 57.62
5e-3	32.75 / 92.88	32.24 / 93.05	32.13 / 92.79	31.37 / 92.68	95.96 / 48.31
1e-2	36.66 / 91.81	30.40 / 93.45	29.47 / 93.54	31.14 / 92.37	88.33 / 86.39
5e-2	31.00 / 93.39	30.88 / **93.46**	30.33 / 92.97	31.43 / 92.50	87.83 / 88.46
1e-1	31.18 / 93.42	33.03 / 93.08	31.71 / 93.17	52.46 / 90.95	95.97 / 53.86
5e-1	35.14 / 92.79	29.55 / 93.34	**29.19** / 93.34	82.19 / 89.22	89.30 / 85.40
1	36.93 / 92.33	34.03 / 93.00	35.45 / 91.74	77.26 / 90.46	97.33 / 48.51
5	31.00 / 93.37	30.48 / 93.37	31.17 / 93.21	83.14 / 89.83	97.43 / 50.74

$\gamma_{\max}=0.5$

β	ρ = 1e-2	1e-1	1	10	100
1e-3	33.10 / 92.59	32.25 / 92.84	30.40 / 92.97	31.70 / 92.39	87.47 / 86.53
5e-3	34.15 / 92.33	31.80 / 92.33	31.97 / 92.49	31.75 / 92.48	90.14 / 86.43
1e-2	34.35 / 92.28	33.90 / 92.29	29.72 / **93.29**	29.66 / 92.75	88.49 / 86.76
5e-2	32.61 / 93.04	33.19 / 92.41	33.73 / 92.23	30.28 / 92.99	84.51 / 88.00
1e-1	33.23 / 92.48	35.78 / 91.90	33.89 / 91.97	75.36 / 90.70	96.66 / 57.33
5e-1	32.48 / 92.33	30.56 / 93.19	32.74 / 92.37	84.06 / 88.13	91.47 / 46.58
1	33.90 / 92.25	32.89 / 92.52	31.26 / 92.89	62.99 / 90.64	88.53 / 87.17
5	32.62 / 92.33	32.60 / 92.48	30.04 / 92.94	71.77 / 90.34	96.58 / 49.03

$\gamma_{\max}=0.1$

β	ρ = 1e-2	1e-1	1	10	100
1e-3	93.84 / 50.41	99.39 / 51.61	76.69 / 89.44	75.19 / 89.36	97.09 / 44.87
5e-3	81.55 / 87.48	80.81 / 88.63	75.63 / 90.32	96.69 / 43.59	96.15 / 50.92
1e-2	95.32 / 51.45	91.92 / 55.05	75.40 / 89.75	96.55 / 45.81	95.24 / 48.11
5e-2	**42.65** / 90.84	93.80 / 45.56	99.58 / 50.06	97.08 / 45.02	83.93 / 87.53
1e-1	95.32 / 51.45	91.92 / 55.05	75.40 / 89.75	96.55 / 45.81	95.24 / 48.11
5e-1	90.51 / 84.74	92.42 / **92.06**	91.78 / 90.73	89.48 / 81.07	94.27 / 59.21
1	81.14 / 90.18	82.34 / 89.98	80.38 / 90.42	88.00 / 53.88	95.43 / 46.75
5	96.57 / 45.61	98.16 / 47.34	100.0 / 49.86	94.89 / 51.80	92.12 / 87.10

Table 10: The hyper-parameter effects of `num_search` on the CIFAR benchmarks.

	0	1	2	5	10	20	50	100	200
CIFAR-10									
FPR95	3.33	2.90	**2.41**	2.61	2.62	2.46	2.74	2.86	3.00
AUROC	98.59	**99.10**	98.96	98.91	98.92	98.56	98.95	99.07	98.80
CIFAR-100									
FPR95	36.47	34.12	33.55	33.30	**30.38**	31.27	32.01	33.07	31.73
AUROC	91.75	92.60	92.98	93.14	**93.62**	93.36	93.18	92.91	93.22

Table 11: The hyper-parameter effects of `ps` on the CIFAR benchmarks.

	$1e^{-2}$	$5e^{-2}$	$1e^{-1}$	$5e^{-1}$	1	5	10	50	100
CIFAR-10									
FPR95	2.97	2.76	2.80	**2.49**	2.57	2.92	3.01	3.04	2.92
AUROC	99.00	**99.02**	98.95	98.94	98.82	98.90	98.97	98.81	98.30
CIFAR-100									
FPR95	35.74	35.75	32.64	**29.00**	31.03	33.63	32.93	37.61	95.07
AUROC	92.82	92.45	93.14	**93.95**	93.18	92.74	92.74	93.09	91.17

F.6 Aligning Training Epochs

In our experiments, we follow the suggested hyper-parameters for the baselines, running OE with 10 epochs on the CIFAR benchmarks. However, our DAL, due to distribution augmentation, is run for 50 epochs to fully fit the augmented distribution. To demonstrate that our improvement is not dominated by longer training time, we also list the results of OE with 50 epochs training, summarizing the results on the CIFAR benchmarks in Table 12. As we can see, although OE can produce better results with 50 epochs of training, our DAL can still demonstrate its superiority in OOD detection. For example, on CIFAR-100, our DAL improves OE by 7.67 w.r.t. FPR95 and 1.92 w.r.t. AUROC.

Table 12: Comparison between OE and DAL with 50 epochs training.

	CIFAR-10		CIFAR-100	
	FPR95 ↓	AUROC ↑	FPR95 ↓	AUROC ↑
OE	3.07	98.97	37.35	92.00
DAL	**2.68**	**99.01**	**29.68**	**93.92**

F.7 Other Norms

We can also use the l_2 norm and the associated Wasserstein-2 distance. Therefore, we conduct the related experiments on the CIFAR benchmarks in comparing between l_1 and l_2 norms, and the results are summarized in Table 13. As we can see, we do not observe an obvious difference between using ℓ_1 and ℓ_2 norms, so it is proper to use the ℓ_1 norm and the Wasserstein-1 distance in our DAL by default.

Table 13: Using ℓ_1 and ℓ_2 norms.

	ℓ_1 norm		ℓ_2 norm	
	FPR95 ↓	AUROC ↑	FPR95 ↓	AUROC ↑
CIFAR-10	**2.68**	**99.01**	2.81	98.98
CIFAR-100	**29.68**	93.92	30.20	**93.95**

F.8 Linear Probing

In many applications, the costs of re-training and re-deployment can be prohibitively high, where we should assume a fixed feature extractor **e** and allow only the classifier **h** (i.e., the fully connected layer) to be tuned. DAL is also adaptable for such a restricted setting, with improved detection performance over the OE counterpart. Table 14 summarizes the results on CIFAR-100, comparing OE and DAL under the settings of full training (fine tuning) and training with only the classifier (linear probe). As we can see, for the linear probe setup, DAL can still improve the OE counterpart, while the performance gain is largely limited compared to that of the full training.

Table 14: Comparison between fully fine-tuning and linear probing.

FPR95 ↓	linear probe	fine tune
OE	50.09	43.14
DAL	**43.37**	**29.68**

F.9 False Negative Rate

We further consider the metric of false negative rate (FNR95) for ID data when the true positive rate of ID data is at 95%. We summarize the results on the CIFAR benchmarks in Table 15, where we consider the common OOD detection setups as in Table 1 and the challenging CIFAR-10 vs. CIFAR-100 setup as in Table 2. As we can see, the FNR decreases for all three considered cases, further demonstrating the effectiveness of our method.

Table 15: Experiments measured by FNR95.

FNR95 ↓	CIFAR-10	CIFAR-100	CIFAR-10 vs. CIFAR-100
MSP	33.02	64.83	43.01
OE	5.04	41.31	26.38
DAL	**3.89**	**26.87**	**22.81**

Table 16: Comparison between our method and advanced methods on ImageNet. ↓ (or ↑) indicates smaller (or larger) values are preferred, and a bold font indicates the best results in the column.

Method	Textures		Places365		iNaturalist		SUN		Average	
	FPR95 ↓	AUROC ↑	FPR95 ↓	AUROC ↑	FPR95 ↓	AUROC ↑	FPR95 ↓	AUROC ↑	FPR95 ↓	AUROC ↑
					Using ID data only					
MSP	66.58	80.03	74.15	78.97	72.72	77.19	78.70	75.15	73.04	77.84
Free Energy	52.84	86.36	70.64	81.67	73.98	75.97	76.92	78.08	68.60	80.52
ASH	15.93	96.00	63.08	82.43	52.05	83.67	71.68	77.71	50.68	85.35
Mahalanobis	40.52	91.41	97.10	53.11	96.15	53.62	96.95	52.74	82.68	62.72
KNN	26.54	93.49	78.64	76.82	75.78	69.51	74.30	78.85	63.82	79.66
VOS	94.83	57.69	98.72	38.50	87.75	65.65	70.20	83.62	87.87	61.36
					Using ID data and auxiliary OOD data					
OE	57.34	82.97	7.92	98.04	73.87	76.94	52.60	77.31	52.60	83.81
Energy-OE	42.46	88.27	1.88	99.49	73.81	**78.34**	69.45	79.54	46.90	86.41
ATOM	60.20	90.60	7.07	98.25	74.30	77.00	55.87	75.80	49.36	85.41
DOE	35.11	92.15	0.72	99.79	72.55	78.00	59.06	85.67	41.86	88.90
POEM	40.80	89.78	0.26	99.70	73.23	68.83	65.45	82.08	44.93	85.10
DAL	55.49	85.29	5.83	99.09	74.23	76.70	50.76	79.21	46.57	85.08
DAL-ASH	**14.10**	**97.00**	**0.23**	**99.85**	**67.38**	78.20	**45.14**	**85.90**	**31.71**	**90.24**
DAL-Energy	33.83	90.44	0.47	99.82	74.37	67.68	49.12	80.28	39.45	84.55

F.10 ImageNet Evaluations

We also conduct experiments on the ImageNet benchmarks, demonstrating the effectiveness of our DAL when facing this very challenging OOD detection task.

OOD Datasets. We adopt a subset of ImageNet-21K-P dataset (Ridnik et al., 2021) as the auxiliary OOD data, which is cleansed to avoid those classes that coincide with ID cases. Furthermore, iNaturalist (Horn et al., 2018), SUN (Xu et al., 2015), Places365, and Textures are adopted as the real OOD datasets, where we eliminate those data whose labels coincide with ID cases.

Hyper-parameter Selection. The hyper-parameters are also tuned on the validation data. We adopt the random search that follows the following three steps. Step 1: we randomly select a hyper-parameter (e.g., β) and fix the values of all other hyper-parameters to be their current optimal values. Step 2: we choose the best β from the candidate set. Step 3: do Steps 1-2 again. We repeat Steps 1 and 2 for 50 times in our experiments. For the backbone model, we use ResNet-50 with the pre-trained parameters published by the PyTorch official repository.

Hyper-parameters Setups. Our DAL is run for 5 epochs. The batch size is 64 for both the ID and the OOD cases. We have the initial learning rate $1e^{-4}$, $\gamma_{\max} = 10$, $\beta = 0.5$, $\rho = 0.1$, and ps = 0.1. Furthermore, we employ cosine decay (Loshchilov and Hutter, 2017) for the learning rate.

ImageNet evaluations. Due to the large semantic space and complex image patterns, OOD detection on the ImageNet dataset is a challenging task (Huang and Li, 2021). However, similar to the CIFAR benchmarks, DAL can also reveal the best detection performance over all the considered baseline methods. Moreover, it is well-known that MSP scoring can easily fail on the ImageNet benchmark (Hendrycks et al., 2022), so we also report the results after DAL training using ASH (DAL-ASH) and Free Energy (DAL-Energy), which can further improve the detection performance.